Modeling identifies chromosome number, size, and non-homologous repulsion as novel determinants of meiotic pairing

Ariana Chriss[1,2†], G. Valentin Börner[2,3*], Shawn D. Ryan[1,4*],

1 Department of Mathematics and Statistics, Cleveland State University, Cleveland, OH 44115
2 Department of Biological, Geological, and Environmental Sciences, Cleveland State University, Cleveland, OH 44115
3 Center for Gene Regulation in Health and Disease, Cleveland State University, Cleveland, OH 44115
4 Center for Applied Data Analysis and Modeling, Cleveland State University, Cleveland, OH 44115

†Current Address: Graduate School of Biomedical Sciences, Icahn School of Medicine, Mount Sinai, New York, NY 10029
* Corresponding Authors: g.boerner@csuohio.edu (GVB), s.d.ryan@csuohio.edu (SDR)

Abstract

Pairing of homologous chromosomes (homologs) is a key feature of multiple cellular processes including gene expression control, chromosome break repair, and chromosome segregation. During meiosis, homolog pairing ensures formation of haploid gametes from diploid precursor cells, a prerequisite for sexual reproduction. Pairing during meiotic prophase I facilitates crossover recombination and homolog segregation during the ensuing reductional cell division. The timing of homolog pairing relative to meiotic recombination and chromosome movements has been determined in several organisms. Yet, mechanisms by which homologs become stably aligned in the presence of an excess of non-homologous chromosomes have remained elusive. Apart from homolog attraction, provided by early intermediates of homologous recombination, disruption of non-homologous associations also appears to contribute to homolog pairing, as suggested by the detection of stable non-homologous chromosome associations in pairing-defective mutants. Here, we have developed an agent-based model for homolog pairing derived from the dynamics of a naturally occurring chromosome ensemble. The model simulates unidirectional chromosome movements, as well as collision dynamics determined by both attractive and repulsive forces. Incorporating natural chromosome lengths, the model accurately recapitulates efficiency and kinetics of homolog pairing observed for wild-type and mutant meiosis in budding yeast. Identification of thresholds for chromosome movement velocity, number, and repulsive forces suggests that collisions between non-homologous chromosomes may contribute to pairing by crowding homologs into a limited nuclear area thereby creating preconditions essential for close-range homolog pairing.

Author summary

Pairing of homologous chromosomes is a key process during meiosis and is shared among all sexually reproducing eukaryotes. Mechanistic determinants of

homology-specific chromosome alignment are presently unknown. We have developed an agent-based model where contributions of the entire chromosome set to the pairing process is taken into account, comprising both homologous and non-homologous chromosomal encounters. Chromosome number and size as well as movement velocity and repulsive forces are identified as key factors in the kinetics and efficiency of homologous pairing. Predictions from the model are readily compared to experimental data from budding yeast, parameters can be adjusted to other cellular systems and predictions from the model can be tested via experimental manipulation of the relevant chromosomal features.

Introduction

Double stranded DNA has an uncanny ability to find a homologous partner in DNA mixtures of staggering complexity. While homologs in somatic cells tend to occupy nuclear areas more distant than expected, somatic pairing nevertheless underlies important biological processes, including X chromosome inactivation and association of loci affected by genomic imprinting [1, 2]. During meiosis, homolog pairing is a key requisite for the separation of homologs to opposite spindle poles during meiosis I. When pairing is compromised, homologs fail to form crossovers, resulting in homolog nondisjunction and the formation of gametes with a surplus or deficit of one or several chromosomes. The resulting chromosomal imbalances are a leading cause for birth defects and still births [3].

In many organisms, meiotic pairing depends on recombination initiation via double strand breaks (DSBs), enzymatically induced by the spo11 transesterase [4]. DSBs typically occur at a multitude of chromosomal positions, at different positions in different cells. DSB processing is closely associated with the homology search, a process whereby 5' resected DNA breaks assess homology between nearby chromosomes at the DNA sequence level [5]. If matched, DSBs are processed via homologous recombination into crossovers as well as other recombination products [6]. Crossovers involve the reciprocal exchange of chromosome arms between homologs at allelic positions [7]. In addition to providing physical linkage between homologs and ensuring their attachment to opposite spindle poles, crossovers also increase genetic diversity [6].

The timing and genetic requirements of homolog pairing have been extensively studied in several organisms [6–10]. In budding yeast, homologs are somatically paired in G1-arrested cells, unpair during premeiotic DNA replication and commence re-pairing as cells initiate homologous recombination [10–12]. Around the time when homolog pairing is established, chromosomes also undergo rapid movements throughout prophase I, as a prerequisite for efficient pairing. Chromosome movements are mediated by the attachment of their ends (telomeres) to cytoplasmic motile filaments [13–15]. Pairing is completed around the time when both DSB ends have undergone strand exchange, giving rise to double Holliday junctions, a critical precursor of crossovers [10, 12]. Both recombination initiation and DSB processing into joint molecules including single end invasions and double Holliday junctions is required for homolog pairing, even though crossover formation itself appears to be dispensable [8, 10, 12, 16, 17].

The synaptocomplex (SC) is a proteinaceous structure that assembles between paired homologs and juxtaposes their axes closely at 100 nm, a distance conserved in most taxa [6, 8–10]. Homologous chromosomes are considered as paired once they have associated at a distance ≤ 400 nm, corresponding to the distance between co-aligned homolog axes in absence of the SC [8].

There are many challenges to experimentally monitor homolog pairing. Fixated, surface-spread cells exhibit superior resolution, but they do not provide insights about chromosome dynamics during the pairing process and nuclear architecture may become

distorted [12, 18]. Tracking of chromosome trajectories in live cells is hampered by limited resolution and potential effects of phototoxicity [19]. Moreover, fortuitous co-localization due to the small dimensions of the yeast nucleus must be taken into account via analysis of non-homologous chromosome pairs [10, 12, 16, 18]. Such studies are further limited to a small subset of chromosomes due to the necessity to fluorescently label individual chromosomes [10, 16, 20].

Little is known about the molecular mechanism(s) of homolog pairing. Several mathematical models have been put forward examining potential contributions of molecular processes to homolog pairing, including telomere attachment to the nuclear envelope, chromosome bending stiffness or polymer chains exhibiting an excluded volume repulsive potential [19, 21–24]. Moreover, a cellular automaton model was developed that examines random searching via chromosome shuffling [25]. Importantly, existing pairing models cannot be validated due to inaccessibility of individual pairing events to experimental analysis. Importantly, existing pairing models cannot be experimentally validated due to inaccessibility of individual pairing interactions to such analyses.

Here, we have developed an agent-based model (ABM), in which movements and interactions initiated by individual chromosomes (i.e. agents) are simulated, thereby recapitulating the interaction dynamics of an entire nuclear chromosome set. Rather than making assumptions about pairing dynamics along individual chromosomes, we use differential equations based on first principles that govern the movements of chromosomes as an outcome of interactions with all other chromosomes within the same nucleus. Our model allows for the analysis of individual trajectories for all chromosomes throughout meiotic prophase I, facilitating comparison with experimental data. Modifications of various chromosomal parameters, including chromosome number, size, and movement velocity as well as attractive and repulsive forces provide insights into the contributions of each of these factors.

Materials and methods

Modeling Approach

Our homologous pairing model considers three contributing processes, i.e., chromosome interactions (homologous and non-homologous collision dynamics), chromosome translation (self-propelled , directed movements), and random chromosome motion (thermal noise within the nucleus) (Fig. 1). By deriving a model entirely from these first principles, we avoid the introduction of mathematical parameters not apparent from the underlying biological process. A key feature of our model is the inclusion of attractive and repulsive forces representing processes that stabilize homologous pairing or disrupt non-homologous interactions, respectively. Rather than focusing on a single homolog pair, our model captures trajectories of complete chromosome sets throughout prophase of meiosis I, facilitating comparison with experimental data and adjustments to species-specific features such as chromosome size and number as well as nuclear dimensions.

To compute the net motion of meiotic chromosome sets, we consider only pairwise interactions between chromosomes as provided by a semi-dilute solution [26, 27]. For the dynamics of the center of mass, $\mathbf{x}_i \in \mathbb{R}^2$, a coupled system of N equations can be proposed as

$$\dot{\mathbf{x}}_i = v_0 \mathbf{d}_i + \sum_{i \neq j}^{N} \mathbf{F}^j(\mathbf{x}_i - \mathbf{x}_j) + \sqrt{2D}\dot{\mathbf{W}}, \tag{1}$$

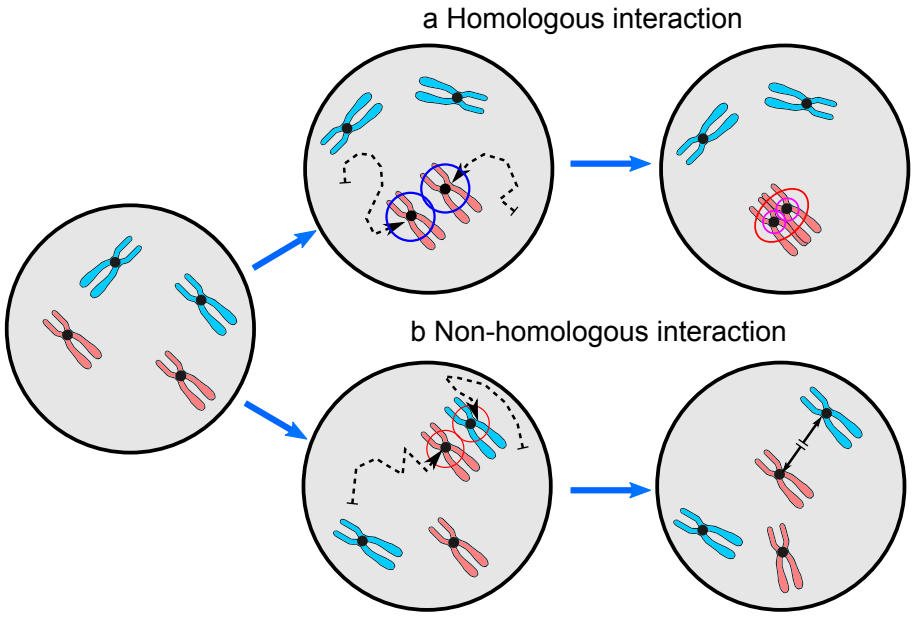

$$\dot{\mathbf{x}}_i = \overbrace{v_0\mathbf{d}_i}^{Translation} + \overbrace{\sum_{i\neq j}^{N}\mathbf{F}^j(\mathbf{x}_i-\mathbf{x}_j)}^{Interaction} + \overbrace{\sqrt{2D}\dot{\mathbf{W}}}^{Noise} \quad (1)$$

$$\mathbf{F}^j(\mathbf{x}_i-\mathbf{x}_j) = -\nabla U(\mathbf{x}_i-\mathbf{x}_j) \quad (2)$$

$$U(\mathbf{x}_i-\mathbf{x}_j) = \begin{cases} C_r e^{-\frac{|\mathbf{x}_i-\mathbf{x}_j|}{\ell_{r_1}}} - C_a e^{-\frac{|\mathbf{x}_i-\mathbf{x}_j|}{\ell_a}}, & j \text{ hom.}, \\ C_r e^{-\frac{|\mathbf{x}_i-\mathbf{x}_j|}{\ell_{r_1}}} + C_r e^{-\frac{|\mathbf{x}_i-\mathbf{x}_j|}{\ell_r}}, & j \text{ nhom.} \end{cases} \quad (3)$$

Fig 1. Determinants of chromosome dynamics during the meiotic homology search. All chromosomes move about the cell nucleus and while searching for their homologous pair perform a continuous random walk (dashed arrows) within the confines of the nuclear envelope (bold circles), with velocity and changes in direction determined by interactions between chromosomes as well as thermal noise. (a) When homologs enter each other's attractive radii of 350 nm (i.e., centers are 700 nm apart), they exert attractive forces (Eq. (3); j hom) on each other which move them closer until they reach their respective exclusive radii (magenta; here 50 nm) keeping them at a constant distance. They subsequently continue their effective "random walk" in a paired status moving as a single non-homologous chromosome pair with respect to all other chromosomes in the nucleus. (b) When a chromosome enters the repulsive radius of a non-homolog (red; here 400 nm), the repulsive force in (Eq. (3); j nhom) diverts their movement at the angle of their encounter with new velocity proportional to the minimum interaction distance (See Figure 3 For illustration, the ring colors match the terms in the Morse potential governing the interactions between chromosomes in Eq. (1)-(3).

where N gives the number of chromosomes and $\mathbf{F}^j$ is the force between two chromosomes, which is obtained as the negative gradient of the potential energy U

$$\mathbf{F}^j(\mathbf{x}_i - \mathbf{x}_j) = -\nabla U(\mathbf{x}_i - \mathbf{x}_j). \tag{2}$$

The potential energy is defined using the Morse potential [28]

$$U(\mathbf{x}_i - \mathbf{x}_j) = \begin{cases} C_r e^{-\frac{|\mathbf{x}_i - \mathbf{x}_j|}{\ell_{r_1}}} - C_a e^{-\frac{|\mathbf{x}_i - \mathbf{x}_j|}{\ell_a}}, & j \text{ hom.}, \\ C_r e^{-\frac{|\mathbf{x}_i - \mathbf{x}_j|}{\ell_{r_1}}} + C_r e^{-\frac{|\mathbf{x}_i - \mathbf{x}_j|}{\ell_r}}, & j \text{ nhom.} \end{cases} \tag{3}$$

Three additional components in Eqs. (1) to (3) are noteworthy. First, there is a translational velocity term ($v_0\mathbf{d}_i$) defining a chromosome's present straight-line motion as one component of its total velocity. We refer to this as the chromosomes translational velocity because it is straight-line motion in the direction the chromosome is already moving and is just one component of a chromosome's total velocity. The velocity (v_0) is multiplied by a chromosome's dimensionless orientation $\mathbf{d}_i = \mathbf{v}_i/\|\mathbf{v}\|_i$, a unit vector in the direction of the chromosome's velocity. $\mathbf{d}_i$ can be changed by collisions with other chromosomes or with the nuclear envelope as well as by thermal noise. In living cells, chromosome movement is typically generated by cytoplasmic motile filaments which are connected to chromosome ends (telomeres) via a protein complex that traverses the semi-fluid nuclear envelope [6, 23, 29, 30]. Chromosome end attachment to the nuclear envelope is reflected in our model by the two-dimensional features of the nuclear volume simulating movement along an invariable z-surface.

Second, interaction forces between chromosomes are captured by Eqs. (2) and (3). The force $\mathbf{F}$ is derived from the potential energy defined by the Morse potential U and is singularly determined by the distance between two chromosomes $\|\mathbf{x}_i - \mathbf{x}_j\|$ [28]. The potential energy between homologous partner chromosomes in Eq. (3) is derived from a Morse potential which is defined as a difference of Yukawa (exponentially decaying) potential energies, assigning a weak attractive force strength C_a to homologous chromosome pairs that models incipient pairing over longer distances (blue ring, here 700 nm; Fig. 1) and a repulsive force strength C_{r1} at short distances ensuring that paired chromosomes are kept at a fixed center-to-center distance rather than overlapping (purple ring, here 100 nm; Fig. 1). Thus, when homologous chromosomes interact, the type of interaction is determined by their distance: namely, attractive around 700 nm and repulsive at 50 nm when homolog pairing has been completed. The potential energy between non-homologous chromosomes is provided by a purely repulsive force (red term in in Eq. (3); see below). Following a non-homologous encounter, chromosomes move away from each other while maintaining their orientation with the new velocity proportional to the interaction distance. Mathematically, the Yukawa potential has a simple formula for its derivative defined in Eq. (2) which gives the corresponding interaction force and allows for straightforward numerical computation. Each of the three forces are at their respective maxima when chromosomal centers of mass overlap, and decrease exponentially from there, falling, e.g., to $\sim 1/3$ of their maxima when their distance has reached the effective radius l_a or l_r respectively. Beyond this effective radius they are essentially irrelevant to chromosome motion because these components of velocity are significant smaller than translation velocity, v_0, or the random motion term. Thus, all of these forces represent short-range interactions that do not affect the motion of a given chromosomes or any other beyond those effective length scales (see Fig. 2).

Third, there is a term in Eq. (1) accounting for thermal noise within the nucleus. This is a small white-noise process where $\dot{\mathbf{W}} \sim N(0, \sqrt{dt})$ can be modeled as a normally distributed random variable with mean zero and variance proportional to the time step. Though the chromosomes are tethered to the nuclear envelope, their motion is not linear

and thermal noise plays an active role at this small scale. This is best modeled as a random walk. Note that the net motion is not that of a random walk, but this component contributes to the overall motion resulting in a more biologically relevant motion. This formulation has been successfully used to capture thermal noise in other models describing microscale biological processes [31–37].

Finally, our approach replaces microscopic details of the physical chromosome shape with a representation of the dynamics of its center of mass, which resembles the green fluorescent protein (GFP) dot in the experimental setting. This allows for chromosome movement to be the direct response of interaction frequencies between homologous and non-homologous chromosomes throughout the nucleus. Our model is simplifying the nucleus from three to two dimensions, providing a direct correspondence to the two-dimensional nature of the experimental data set used to calibrate the model where biological sample preparation involves flattening of the nucleus [12]. Finally, our modeling framework treats homolog pairing as an endpoint and does not consider the ensuing homolog segregation during meiosis I, again facilitating comparison to experimental data where cells are arrested at the pairing stage due to absence of meiotic progression factor Ndt80 [12, 16].

Parameter Choice

While our model is adaptable to a wide range of parameters, it is important to identify realistic values for comparison with specific experimental data. Table 1 displays the parameter values used in initial simulations. Meiosis in the budding yeast *S. cerevisiae* (the organism from which the experimental data set used for model calibration was obtained) involves 16 homolog pairs or 32 individual chromosomes, corresponding to 32 equations, each simulating the dynamics of the center of mass for an individual chromosome. Chromosomes may come in close contact with the nuclear boundary without ever crossing it due to an appropriate value set for the boundary repulsion strength and characteristic length scale using a purely repulsive Morse potential. While the intact yeast nucleus is roughly 2μm in diameter, it is set here to 6.5μm to account for its flattening during experimental data collection [5, 12]. This is critical for direct comparison with recent experimental results to establish model validity. These flattened nuclei result in chromosome motion primarily in the two-dimensional cross-section shown in Figure 1. We emphasize again that the chromosomes are still tethered to the nuclear membrane, and the simulation effectively tracks the chromosome movement in this two-dimensional cross-section. Experimentally determined distances between GFP-tagged chromosomes range between 200 nm (the resolution limit of light microscopy) and 6.0μm [12].

Attractive and repulsive interactions between homologous and non-homologous chromosomes, respectively, are presently not accessible to measurements, but their length scales can be estimated from features that have been determined in several biological systems. Many of these interactions involve evolutionarily conserved components of the homologous recombination machinery for which measurements are available [6]. Attractive forces likely correspond to forces exerted by the additive effects of resected DSBs that succeed in forming D-loops with intact homologous chromosome segments [6]. Repulsive forces arise when the nascent interactions between non-homologous chromosomes are disrupted, possibly during heteroduplex rejection of an invading DSB by the mismatch repair machinery and/or by other chromosomal components normally involved in preventing associations between non-homologous chromosomes (see Discussion; [38, 39]). Parameters also need to reflect features of the decision process whether or not two chromosomes are homologs (e.g., parameters should not result in chromosomes jumping apart or allow overlap or prolonged association of non-homologous chromosomes).

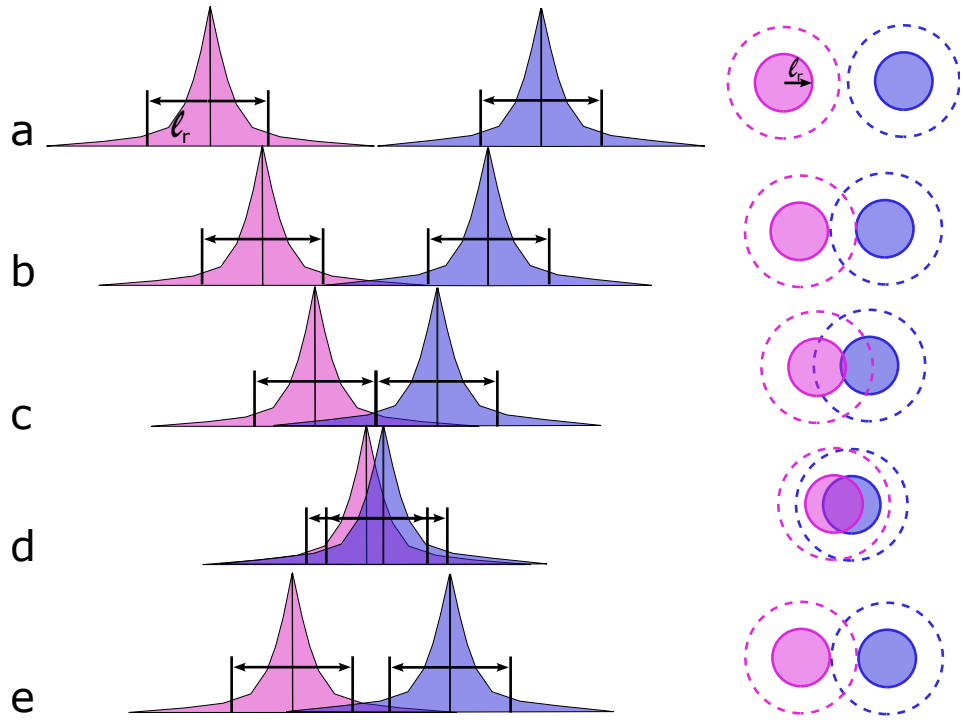

Fig 2. Strength of exponentially decaying repulsive forces between non-homologous chromosomes (a-e) Illustration of exponentially decaying repulsive force when two non-homologous chromosomes meet. The vertical black line represents the center of mass, $\mathbf{x}_i$, and the colored regions indicate each chromosome's repulsive force modeled as a decaying exponential. The solid circles on the righthand side indicate the effective repulsive radius (see Table 1) beyond which the force is considered negligible. The dashed radii indicate the attractive region which plays no role in a non-homologous interaction. The repulsive force felt by a participating non-homologous chromosomes corresponds to where the center of mass crosses into the other chromosome's repulsive region. Observe that the net effect has a very short range and chromosomes must be very close to have their motion influenced by the repulsive interaction force. See also Fig. S4 Fig and Supplemental Movie S1.

The attractive length radius (l_a) is set to 700 nm corresponding to approximately 1,400 nucleotides of fully extended, single stranded DNA (assuming 0.50 nm/bp; [40, 41]). During the homology search, such 5' resected DSB tentacles may reach out from the broken chromosome to other chromosomes to probe homology [9]. Thus, two chromosomes with centers of mass within 700 nm will initiate the homology search. When chromosomes are homologous, they are moved toward one another by the attractive force. As homologs get closer, the repulsive force ensures the binding distance/excluded volume halts them at a distance of 50 nm which approximately corresponds to the conserved 100 nm width of the synaptonemal complex [6]. Once homologs are paired, they remain so henceforth and assume a single equation of motion ensuring they do not break apart.

The repulsive length (l_r) is set to a 400 nm center of mass radius based on the following considerations: First, homologs are considered as paired when they are coaligned at a distance of approximately 400 nm, the distance between paired but unsynapsed homolog axes [8]. The detection or rejection of homology likely involves overlapping processes, further suggesting that interactions at similar length scales contribute to both outcomes. Thus, we choose 400 nm as the distance needed to determine if an approaching chromosome is non-homologous. Second, collisions promptly dissociate non-homologous chromosomes ensuring that they do not persist at distances below 400 nm. We note that the model uses only a short-range repulsive interaction that only becomes significant when the chromosome centers of mass are less than 400 nm apart, thus resulting in essentially no effect on chromosomes beyond this range (Fig. 3; for details see Fig. S4 Fig).

Our choice for the strengths of homologous and non-homologous interaction forces is further motivated by kinetic considerations. Non-homologous interaction strength is directly related to the time spent exploring that interaction by a given chromosome. Thus, the repulsive force strength, C_r, is chosen larger than the attractive strength, C_a, thereby shortening the time spent by non-homologous partners with each other. By contrast, the interaction between homologous chromosomes requires a longer time period for the assessment of homology. Notably, doubling the repulsive strength cuts the time spent in proximity in half for non-homologous chromosomes (Compare Figs. S4 Fig-S5 Fig).

Apart from collisions, the homology search involves the following processes. Directed, long-range chromosome movements increase the probability of chromosomal encounters allowing them to probe homologous and non-homologous DNA partners. The velocity of chromosome movements at 300 nm/s is taken from live-cell imaging of meiotic chromosome movements which range between 200 and 500 nm/s [14, 15, 29]. Notably, chromosomal encounters are enhanced by prophase I chromosome movements, whereas an attractive volume with 700 nm radius without movements would limit the homology search for a given chromosome to approximately 5% of the nuclear area [42]. The parameter for chromosome motion due to thermal noise is provided from the diffusion constant of interphase chromatin which ranges between 10^2 and 10^3 nm^2/sec [43].

At the start of each simulation, chromosomes are assigned unit velocities and random initial placements throughout the nucleus using a basic exclusion algorithm where a chromosome is placed and then its center of mass distance to all other chromosomes previously placed is computed [21]. If any initial distance is below 700 nm indicating pairing, another random location is chosen for the respective chromosome to avoid overlap in the initial chromosome placement, repeating this process until all chromosomes have been placed. The choice of 700 nm is conservative, and the model is easily adaptable to alternative initial placement exclusion distances.

Table 1. Table of parameters used in the simulations. Movement speed for *spo11* hypomorph from [14]

Parameter	Dim. Value	Nondim. Value		
		Base	*spo11*(i)	*spo11*(ii)
Nucleus (domain) radius L	3.25 μm [12]	3.25	3.25	3.25
Effective chromosome length L_e	1 μm [15]	1	1	1
Diffusion constant D	10^2nm^2/s [43]	0.0001	0.0001	0.0001
Movement speed v_0	300 nm/s [29]	0.3	0.231	0.3
Length scale, attractive force ℓ_a	700 nm (Est.)	0.7	0.7	0.7
Length scale, repulsive force (non-hom. chromosomes) l_r	400 nm [8]	0.4	0.4	0.4
Length scale for repulsive force (hom. chromosomes) l_{r_1}	50 nm [6]	0.05	0.05	0.05
Attractive Strength C_a	N/A	0.003	10^{-7}	.0009
Repulsive Strength for non-hom. chromosomes C_r	N/A	0.05	0.05	0.015
Repulsive Strength for homologous chromosomes C_{r1}	N/A	0.05	0.05	0.015
Boundary repulsion strength C_b	N/A	0.5	0.5	0.5
Boundary repulsion length ℓ_b	N/A	0.05	0.05	0.05

Results

Initial model and comparison with experimental data

In the reference experiment, homologous and non-homologous chromosome interactions were monitored by retrieving cell aliquots from semi-synchronous meiotic cultures which either carry two GFP-tagged copies of chromosome III or single copies of GFP-tagged chromosomes III and II, to monitor homologous or non-homologous chromosome interactions, respectively [12]. Pairing was inferred from the frequency of cells with GFP dots separated by less than 400 nm in the strain carrying GFP-tags in homologous chromosomes adjusted for fortuitous co-localization as derived from measurements in the strain carrying GFP-tags in non-homologous chromosomes pairs. This analysis suggested that homolog pairing is at a minimum around t = 3h after transfer to meiosis medium, during pre-meiotic S-phase, and reaches maximum levels at $t = 7.5h$, when most cells have entered the pachytene stage [12].

To model the complete homology search process throughout prophase I, we simulated chromosomal dynamics using Eq. (1)-Eq. (3). The numerical approach was designed in MATLAB [44]. A base code for the wild-type dynamics is available at [45]. Importantly, the simulation allows concurrent tracking of all 16 homolog pairs and comparing their pairing dynamics to appropriately matched non-homologous partners within the same nucleus, in a large number of realizations. Typically 200 realizations were considered by running Monte Carlo simulations with up to $N = 32$ chromosomes. We began assessing the validity of our model under the simplification that all chromosomes are of uniform length (1μm), corresponding to the measured length of a mid-sized yeast chromosome at the pachytene stage [15].

We initially modeled pairing with a minimum set of two pairs of homologous chromosomes and subsequently increased the number of chromosome pairs to 16. Homologs were considered as paired when they became stably juxtaposed at 400 nm (above). Exploring pairing dynamics in dilute (4 pairs or less) to semi-dilute (more than 4 pairs) conditions, we then determined the maximum pairing efficiencies and pairing kinetics as indicated by the time needed to achieve 50% of maximum homolog pairing. These studies revealed unexpected effects of chromosome numbers on the efficiency and

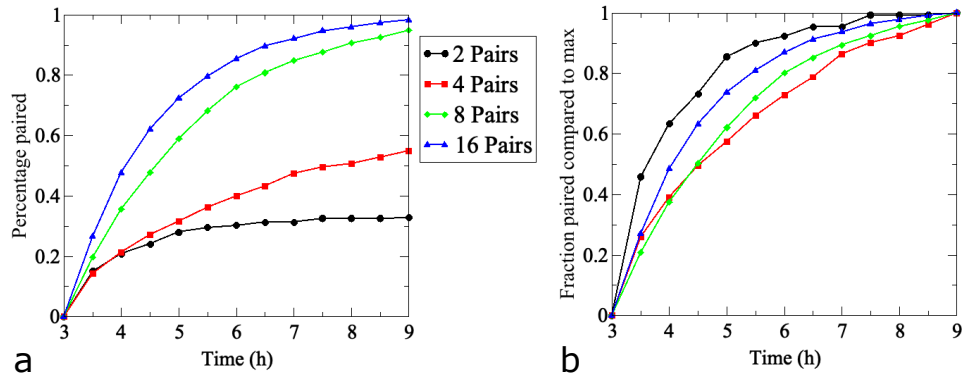

Fig 3. Effects of chromosome number on pairing efficiencies and kinetics. Pairing frequencies for the indicated number of homolog pairs in 200 realizations are combined to compute the percent of homologs paired at the indicated time points. (a) Average pairing levels of the indicated number of equally sized homolog pairs. Error bars are omitted for clarity. (b) Pairing kinetics were determined by normalizing results in (a) as a percentage of maximum pairing levels.

kinetics of pairing.

The model was started at the $t = 3h$ time point, corresponding to minimum pairing levels in the experimental data set. Initial distances range from 700 nm to 6μm (Fig. 3a). For up to 4 homologs, less than half of homolog pairs have completed pairing by $t = 7h$, and increases at later times are negligible. Surprisingly, an increase of homolog pairs to 8 or 16 results in a substantial increase in maximum pairing levels. Accordingly, with ≥ 8 homolog pairs, essentially all homologs have completed pairing by $t = 7h$. Not only the maximum pairing levels, but also the pairing kinetics are accelerated with increasing chromosome numbers. Thus, with 16 homolog pairs, half-maximum pairing levels are achieved by $t = 4h$ compared to $t = 4.5h$ with 4 or 8 homolog pairs (Fig. 3b). (Note that apparent faster pairing kinetics of two homolog pairs are misleading as they arise from the subset of realizations where random placement put homolog pairs in close vicinity facilitating rapid completion of pairing. Yet, in the majority of realizations, homologs are initially further apart, and pairing is never completed resulting in low overall maximum pairing levels). In summary, in the dilute scenario, isolated movements without chromosome interactions are predominant, whereas in the semi-dilute scenario chromosome interactions dominate motion.

Having established that chromosome number affects both pairing efficiency and kinetics, we next explored additional features of the scenario with 16 homolog pairs, i.e. the chromosome set in budding yeast cells. In this analysis, homolog pairs were arranged based on their initial distances in ascending order. Homolog distances were then recorded over time and plotted at four time points corresponding to those determined experimentally for chromosome III (Fig. 4a). Each data point represents average distances from 200 realizations.

Modeling suggests that chromosomes initially separated by 0.7μm to 4μm have completed pairing after less than 2 hours (by $t = 5h$), whereas chromosomes separated by a larger distance require up to 6 hours to complete pairing (Fig. 4a). These results suggest a non-linear relationship between initial homolog distance and pairing kinetics. Moreover, there appears to be a critical initial distance threshold above which homolog pairing becomes very slow.

Distances between non-homologous chromosome partners were also monitored in the same simulation. Data points in this case represent any non-homologous chromosome initially placed at the same distance as the homologous partner chromosome in the same

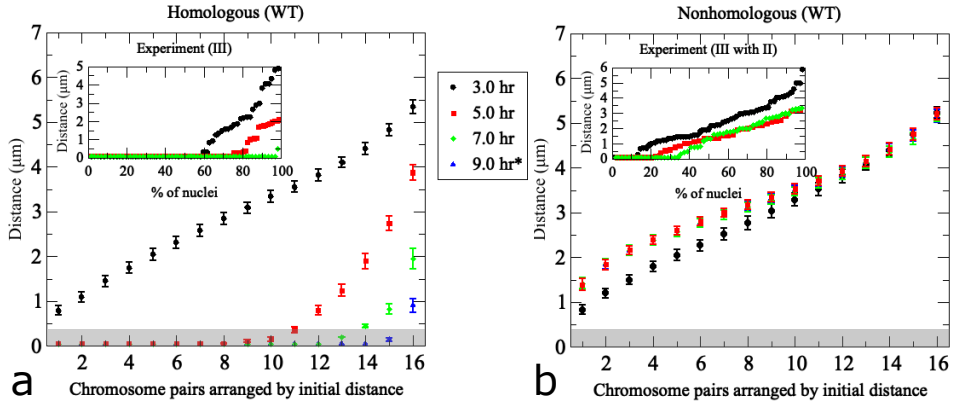

Fig 4. The pairing model captures experimentally determined association kinetics between homologous and nonhomologous chromosomes during wild-type meiosis. (a) Modeling of pairing between 16 uniformly sized partner chromosomes. For each modeling run, chromosome distances at $t = 3h$ are used to uniquely index homologous chromosome pairs, which are arranged based on ascending initial distances along the x-axis. The y-axis indicates average distances from 200 realizations of the agent-based model Eq. (1) – Eq. (3) at the time points indicated by the color code. Error bars indicate standard deviations. The maximum pairing distance of 400 nm is highlighted by a gray rectangle. The inset shows experimentally determined distances between a single pair of GFP-labeled yeast chromosome III measured in a synchronous meiotic culture in fixated nuclei ($n > 100$) (data from [12]). Nuclei are arranged based on distances between homologous GFP signals at a given time point. Note that x-axes are different in the inset due to the fact that in the experiment cells were observed at a given time point and then discarded, whereas in the simulation the same cell was tracked over time. (b) Results from modeling of distances between non-homologous chromosome pairs in the same nuclei analyzed in (a). For non-homologous pairs, each homolog partner is matched with a non-homologous chromosome that at $t = 3h$ exhibits a distance optimally matched to that with its cognate homolog partner . Inset (b) shows experimentally determined distances between non-homologous GFP-tagged budding yeast chromosomes II and III (error bars indicate SD). For details on experimental conditions see (12). The pairing distance is highlighted in gray at 400 nm. *Note the experimental data do not include information for $t = 9h$.

nucleus (Fig. 4b). Accordingly, initial distances between non-homologous and homologous pairs are similar, yet homologous distances become progressively smaller, whereas non-homologous distances remain unchanged over time. Thus, the simulation is indeed specific for homologous pairing.

Comparison between simulation and experiment indicates good qualitative and quantitative agreement in homologous and non-homologous association kinetics (see insets Fig 4). Notably, however, modeled pairing kinetics are derived from the entire set of 16 homolog pairs within the same nucleus whereas experimental data represent distances between a single GFP-tagged chromosome with its homologous partner and a single representative non-homologous partner, measured in nuclei derived from different aliquots and from different cultures. Several additional differences between experimental data and modeling are noteworthy.

First, at the time of transfer to meiosis medium, homologs are paired at high frequencies in G1-arrested yeast cells and undergo unpairing during premeiotic S-phase in a semi-synchronous manner [10, 12]. Accordingly, even at the time of minimum

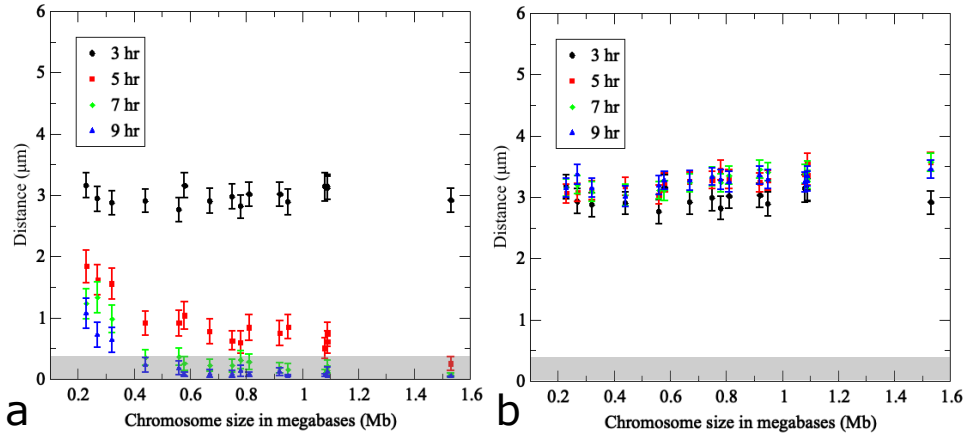

Fig 5. Effects of chromosome size on pairing kinetics and efficiency. (a) Average distances over time between homolog pairs where repulsive and attractive radii are adjusted proportionally to the sizes of actual yeast chromosomes. Note that the three smallest homolog pairs are markedly slower in achieving pairing than all other chromosomes. (b) Non-homologous chromosomes equidistant to each of the two homologs were identified at $t = 3h$ and their distances were monitored throughout the simulation in the same set of model nuclei monitored in (a). (200 realizations, error bars indicate SD). The gray rectangle highlights pairing distances at or below 400 nm.

pairing levels, a substantial subset of cells exhibits homologous pairing (see insets of Fig. 4), either because they are still somatically paired or because they have already progressed to post-replicative pairing. By contrast, homolog pairing at $t = 3h$ was absent in the model due to the initial randomized placement algorithm.

Second, an overlap of homologous GFP signals may occur due to pairing, but also due to coincidental co-localization. For example, during experimental flattening of the nucleus, unpaired homolog pairs may end up in close vicinity and be scored as paired, even though this close vicinity may not have existed when the nucleus was in its original 3D state. Accordingly, non-homologous GFP signals overlap coincidentally in some nuclei, even though they are not paired. This limitation is further emphasized by apparent pairing at substantial frequencies between non-homologous chromosomes (see inset Fig. 4b). Importantly, non-homologous GFP signals remain at similar distances throughout meiosis in both experiment and simulation, with little changes in inter-chromosomal distances. We conclude that the modeling framework reasonably recapitulates the chromosome dynamics associated with homologous pairing throughout prophase I.

0.1 Modeling predicts delayed pairing for the three smallest yeast chromosomes.

The 16 budding yeast chromosomes range in length from 250 kilobasepairs (kbp) to 1,500 kbp. Chromosome size affects several meiotic processes, including the timing and/or density of initiating DSBs and crossovers [46, 47]. Chromosome length may further affect the cumulative range of attractive and repulsive forces as well as the available space for other chromosomes to move in [48]. We therefore took the length of yeast chromosomes into account by scaling all attractive and repulsive radii. The larger area takes into account the higher number of DSBs engaged in the homology search along a larger chromosome, even though the reach of an individual DSB would likely remain unchanged as it is determined by its resection tract length. The inner repulsive

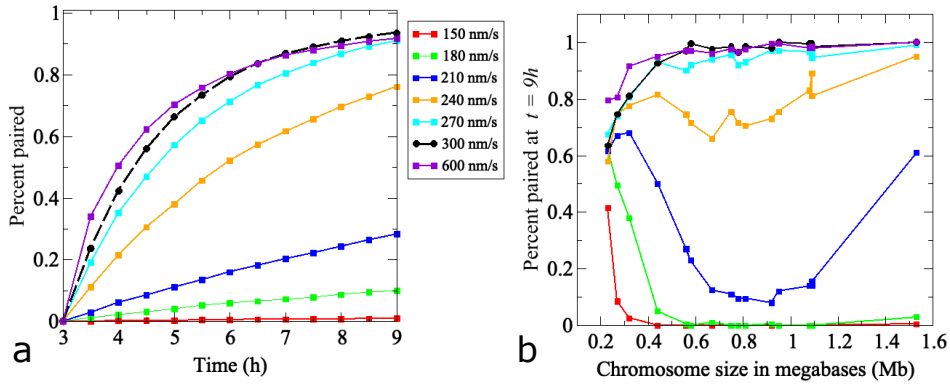

Fig 6. Modeling identifies a critical threshold of chromosome movement velocity for efficient homolog pairing. (a) Dots indicate the average pairing levels over time of all 32 true-sized chromosomes. Black indicates the velocity of chromosome movements in the wild-type model in Figs. 4 and 5 (300 nm/s). Chromosomes fail to pair at velocities around 150 nm/s. Increases in 30 nm/s increments improve pairing efficiencies at $t = 9h \sim 3$-fold, with more modest gains above 240 nm/s where essentially all 16 homologs pair efficiently. For a more detailed analysis of pairing kinetics of (a) see Fig. S1 Fig. (b) Effects of movement velocity for different chromosome sizes. The graph shows pairing levels of chromosomes of increasing sizes at $t = 9h$, indicating that pairing efficiencies of larger chromosomes are more dramatically affected by changes in velocity than those of smaller chromosomes. Note that at higher velocities, chromosomes move further into the repulsive radii of their non-homologous partners and are therefore repelled faster, resulting in an accelerated homology search.

radius enforcing binding distance between homologs were kept at 50 nm, independent of chromosome length, consistent with the uniform width of the synaptonemal complex.

As before, distances between homologous chromosomes were plotted as a function of time, but results were sorted by increasing chromosome lengths rather than by initial chromosome distance (Fig. 5a). For one of the realizations of the entire homology search process of size-adjusted homolog pairs, see Supplementary Movie S1 (`https://zenodo.org/record/7415620#.Y82hJi-B2fV`). In the movie, it is apparent that homologous chromosomes may remain closely aligned for extended periods, but do not complete pairing at that time, e.g., because of repulsive interaction with a non-homologous chromosomes. Such dynamics may explain the mixed association previously observed where homologs approach for 30 min and separate for 30 minutes without completing pairing [19]. Again, initial chromosome distances are on average 3μm for all chromosomes, independent of chromosome length, corresponding to half of the diameter of the cell nucleus. As time progresses, chromosomes longer than 400 kbp have completed homologous pairing by $t = 7h$ in essentially all nuclei, whereas the three shortest homolog pairs which range between 250 and 320 kbp remain unpaired, even at $t = 9h$, as suggested by their final distances of > 700 nm (Fig. 5; pairing distance of 400nm). Thus, the three shortest chromosomes take substantially longer to pair than the rest of chromosomes, revealing a nonlinear effect of chromosome length on pairing kinetics. Importantly, these distinct kinetics are limited to small homologous chromosome pairs, whereas no special features are observed for interactions between the three smallest chromosomes and equidistant non-homologous chromosomes in the same nuclei (Fig. 5b). Hence, our model predicts that smaller chromosomes exhibit unique pairing properties.

Effect of chromosome velocity on pairing

We next used our model to examine the role of chromosome translation velocity, v_0, on pairing efficiencies and kinetics. Even though faster chromosome movements would be expected to uniformly accelerate homolog pairing, these simulations identified a velocity threshold for pairing, which particularly impacts larger chromosomes. In the simulations described previously, the velocity parameter in Eq. (1) was set to $v_0 = 300$ nm/s (see Table 1). Reducing the chromosome translation velocity by 50% (to 150 nm/s) essentially eliminates pairing when average pairing frequencies for size-adjusted chromosomes were monitored over time (red line; Fig. 6a). Increasing chromosome velocity in 30 nm/s increments to 210 nm/s results only in minor increases in pairing efficiencies, with on average only 30% of homolog pairs achieving pairing by $t = 9h$ (Fig.6(a), blue). Surprisingly, the four smallest chromosomes (sized below 500 kbp) disproportionately contribute to pairing at velocities up to 210 nm/s, whereas pairing is essentially abrogated for mid-sized and larger chromosomes (Fig. 6(b); for the exception of the largest 1,500 kb chromosome see below). When chromosome translation velocity is further increased by 30 nm/s to 240 nm/s, this results in a dramatic improvement of pairing efficiency for all chromosomes, with now 80% of homolog pairing completed by $t = 9h$, regardless of chromosome size (orange; Fig. 6). Pairing efficiency and kinetics can be further improved for all chromosomes by an increase of velocity to 270 nm/s (light blue), yet neither a further 30 nm/s incremental increase nor a doubling in chromosome velocity to 600 nm/s has substantial effects on pairing kinetics or efficiency (Fig. 6a; black and purple).

Thus, instead of a linear relationship between chromosome velocity and pairing, our model predicts a threshold effect where velocities above 240 nm/s dramatically improve pairing, a threshold that particularly impacts pairing of mid-sized and larger chromosomes. Surprisingly, the largest chromosome is predicted to behave differently in this respect, exhibiting a dependency on movement velocity much more akin to the smallest chromosomes. This unique behavior may be explained by the large repulsive radius of the chromosome pair relative to the size of the nucleus which likely passively restrains their movements to a shared nuclear territory. The largest chromosome may either start near its homologous partner, making it difficult for the largest chromosomes to reach each other due to restricted zones created by non-homologous chromosomes. Accordingly, at 210nm/s, roughly half of the largest chromosomes are paired, and half are not.

Together, these findings suggest that at velocities below 240 nm/s, repulsive interactions between non-homologous chromosomes are less frequent, diminishing effects of excluded regions defined by the presence of non-homologous chromosomes. Moreover, at lower translational velocity, contributions from random diffusion become more pronounced, interfering with directional chromosome movements. As random motion becomes dominant over directed movement, chromosomes explore less nuclear area, making homologous encounters less likely.

Contributions of attractive and repulsive strength to homolog pairing

Next, we used the model to investigate contributions of attractive and repulsive forces to pairing dynamics. Contrary to expectation, these simulations indicated a more pronounced role of repulsive compared to attractive forces. Fig. 6 compares the base model with both attractive and repulsive forces carrying size-adjusted chromosomes and translation velocities of 300 nm/s (Fig. 7a), with the attractive (purple) or repulsive (blue) term in Eq. (3) set to 0, respectively (Fig. 7b,c). Unexpectedly, these simulations indicate that without attractive forces pairing proceeds with essentially normal

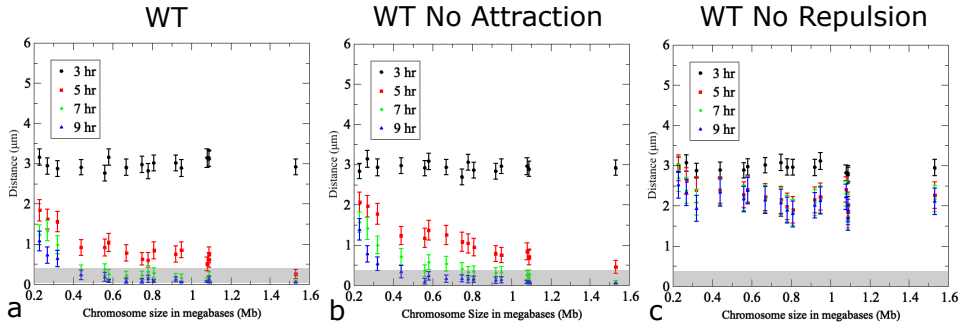

Fig 7. Contributions of attractive and repulsive forces on pairing efficiencies and kinetics. (a) Pairing wild-type model using true chromosome lengths and a standard translational movement velocity of 300 nm/s as primarily studied herein. In (b) the attractive zone is removed by setting the attractive strength $C_a = 0$. In (c) the repulsive force between non-homologs is removed by setting the repulsive strength $C_r = 0$ (200 realizations, error bars indicate SD). The pairing distance is highlighted by a gray rectangle.

efficiencies and kinetics, whereas, the absence of repulsive forces, essentially eliminates pairing for chromosomes of all sizes.

To address this surprising prediction, we examined whether pairing dynamics can be adequately predicted with stronger attractive forces between homologs and weaker repulsive forces between non-homologs (see Fig. S6 Fig). Yet, using these parameters, homologs complete pairing on extremely short time scales that fail to match experimental data. Importantly, the three smallest chromosomes fail to pair altogether, making this scenario less likely.

Adaption of the pairing model to a mutant with reduced DSBs

Building on the expanded model that takes chromosome sizes and optimized velocities into account, we next investigated the case of a meiotic mutant for which experimental data are available [12]. Absence of meiotic DSBs, e.g., in a *spo11* null mutant largely abrogates homolog pairing, consistent with a central role of recombination intermediates in establishing and/or stabilizing homolog pairing [10, 16, 20]. A decrease of initiating DSBs to around 30% of wild type in a hypomorphic *spo11* mutant (*spo11-HA/spo11-HA-Y135F*; hereafter *spo11-HA/yf*) results in delayed, though largely efficient pairing [12]. Model parameters were adjusted to accommodate the fact that reduced DSB abundance would likely reduce the cumulative attractive force exerted by these intermediates [9]. Furthermore, chromosome translation velocity was reduced consistent with experimental data that indicate a reduction of the average chromosome velocity in a *spo11* null mutant by 20% (to 110 nm/s from 140 nm/s in wild type; see Fig. 4A in [14]). Accordingly, for the *spo11* hypomorph, we reduced the attractive strength C_a in magnitude from 10^{-3} to 10^{-7} and the chromosome translation velocity from 300 nm/s to 230 nm/s.

Actual chromosome sizes were used for this simulation, yet results were plotted based on initial chromosome distances to facilitate comparison with the experimental data set in both wild-type *spo11* (Fig. 8a) and *spo11* hypomorph (Fig. 8b-c). We considered two parameter sets to model the *spo11* hypomorph. In the first scenario, both the movement speed and attractive force strengths were reduced to represent the mutant strain's decrease in DSBs available for the homology search as well as slower chromosome velocity (Fig. 8b). In the second scenario, we considered exclusively the DSB reduction in *spo11-HA/yf*, but kept the chromosome movement speed at wild-type

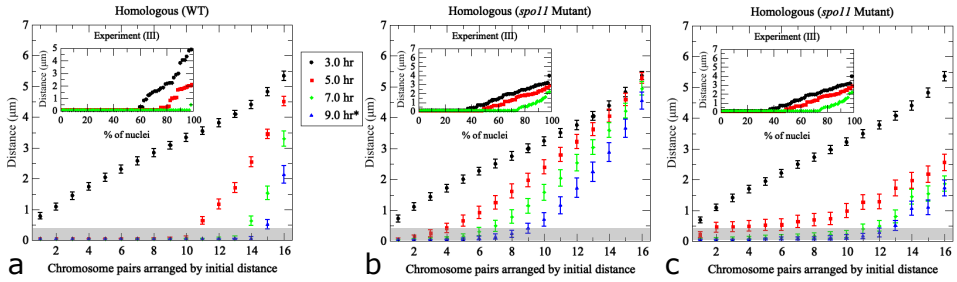

Fig 8. Modeling of pairing kinetics at reduced DSB abundance. (a) Wild-type model with true-sized chromosomes. Results differ from Fig. 4(a) due to use of true sized rather than uniformly sized chromosomes. The inset shows experimental data for yeast chromosome III in hypomorphic *spo11-HA/yf*. Note the x-axis in the inset shows different nuclei derived from aliquots at the indicated time points, whereas the same cells were tracked through time during simulations. (b) Model for *spo11* hypomorphic mutant with reduced movement speed and attractive force strength, with experimental observations for *spo11-HA/yf* shown in the inset. Translational movement velocity is reduced to 77% of wild type levels (230 nm/s), consistent with slower chromosome movements observed in *spo11* (13), and attractive force is reduced 10^4-fold representing decreased attractive forces exerted by fewer DSBs (see Table 1). (c) Alternative model for hypomorphic *spo11* with 3-fold reductions of the wild-type levels of both attractive and repulsive force. For non-homologous chromosome distances see Fig. S3 Fig. The pairing distance is highlighted in gray at 400 nm. (200 realizations, error bars indicate SD).

levels. Since DSBs would likely play a role in generating both attractive and repulsive events, both forces were reduced to 30% of the wild-type value (Fig. 8c). For a specific realization of the homology search in mutant spo11, see Supplementary Movie S2 (`https://zenodo.org/record/7415620#.Y82hJi-B2fV`). While reducing both movement speed and attractive forces delays pairing of widely separated homolog pairs indefinitely, reducing both attractive and repulsive contributions affects all chromosome distances similarly. Importantly, these responses demonstrate the versatility of our model to predict potential contributions of various parameters on pairing dynamics.

Discussion

How homologs pair during meiosis in the presence of an excess of non-homologous chromosomes is presently unknown. We have explored contributions to the pairing process by developing an agent-based mathematical model that simulates homologous pairing accounting for chromosome number, length, as well as attractive and repulsive forces. Our simulations suggest that chromosome movements together with repulsive forces are the key determinants of bringing homologs in close vicinity. Chromosome movements in combination with repulsion create excluded regions within the nucleus, driving homologs into pairing interactions. Repulsive forces are most efficient when chromosome numbers rise above a certain threshold, likely by reducing the available area per nucleus. Attractive forces come into play once distances between homologs are sufficiently small (i.e., less than 1μm), as indicated by progressively shorter distances between homologs in absence of repulsive forces (compare Fig. 5b to 7c). Such close-range homologous pairing interactions have been captured by earlier modeling [19].

The agent-based modeling framework developed here is new to chromosome dynamics but has been useful in modeling other multicomponent systems that involve

attractive and repulsive forces, ranging from molecular to macroscopic components [21, 22, 27, 49–59]. Earlier modeling approaches of homolog pairing have focused on predicted characteristics of individual chromosomes during the pairing process but have not considered the effects of non-homologous chromosomes within the nucleus [19, 21–23].

The introduction of a repulsive force that simulates time constraints on non-homologous interactions is a key feature of our mathematical pairing model. While more pronounced contributions to pairing of repulsive compared to attractive forces may appear counter-intuitive, several mutant phenotypes support a role of interchromosomal repulsion. First, in absence of the dimeric protein complex Hop2/Mnd1, synapsis occurs between non-homologous chromosomes in yeast, mammals and plants [39, 60–63]. While the Hop2/Mnd1 complex also mediates homologous strand exchange [64], elimination of non-homologous interactions likely represents a distinct function of this complex, as non-homologous synapsis is not a universal feature of mutants defective for strand exchange [39]. Repulsive and attractive forces may thus be exerted by a partially overlapping set of proteins. Second, mutation of the Ph1 locus results in erroneous stabilization of interactions between non-homologous chromosomes in allopolyploid wheat, suggesting that Ph1 normally mediates dissolution of such interactions [65]. Third, disruption of recombination between DNA segments with limited sequence similarity by the mismatch repair machinery involves ejection of the invading strand thereby minimizing the association time of non-homologous chromosome partners [38, 39, 66]. In our model, this minimization of association time is simulated by the repulsive force. Finally, in many organisms, homologs enter meiosis separated by distances that far exceed the reach of resected DSBs that could assess homology. This necessitates a process that ensures initial homolog co-localization potentially provided by non-homologous repulsive forces.

Repulsive interactions may also be the underlying cause for temporal separation of paired chromosomes observed in live-cell imaging studies [19]. Temporal separation of homologs has been interpreted and modeled as spatially restricted sub-diffusion involving fully paired homologs [19]. Movie animations of our model indicate that similar disruptions may also arise due to collisions with non-homologous chromosomes of homolog pairs undergoing incipient pairing interactions (see Supplemental Movies S1 and S2). Notably, our model suggests that during this exploratory phase, homolog pairs are susceptible to becoming dislodged due to collisions with non-homologous chromosomes.

Our model has identified unexpected threshold effects for several parameters where minor changes result in major non-linear effects. Accordingly, for the current setting, homologous pairing levels and/or kinetics are disproportionately increased when the chromosome number is increased from 4 to 8 (Fig. 3), when chromosome size exceeds 400 kbp (Fig. 5), and when chromosome velocity is increased from 210 nm/s to 240 nm/s (Fig. 6). Such discontinuities are likely related to a critical threshold of chromosome encounters that needs to be crossed for homologous chromosomes to become confined to the same nuclear areas, thereby facilitating homolog encounters. Accordingly, when chromosomes are present in lower numbers, exhibit smaller sizes or fail to achieve unidirectional movement due to disturbance by Brownian motion, the frequency of non-homologous interactions is reduced and crowding of homologous chromosomes into the same nuclear area occurs at low frequencies.

Rapid chromosome movements during prophase of meiosis I have been observed in species from yeast to mouse [14, 15, 67]. Intriguingly, in different taxa, chromosome movements are mediated by different cytoskeleton components potentially resulting in a wide variation of movement speeds [29]. Our model indicates that chromosome movements must occur above a certain threshold providing a potential reason why

chromosomes move at certain speeds. Moreover, our model predicts that the three smallest yeast chromosomes would be slower in completing homolog pairing (Fig. 5). Notably, the same chromosomes exhibit increased DSB and crossover frequencies [46,47], features that may specifically compensate for size-related disadvantages in pairing.

A key feature of the current agent-based modeling is that all participating entities are included in observations, allowing for the ability to capture both typical behavior and deviations thereof. Experimental analysis of homolog pairing is limited by the availability of distinct tags for individual chromosomes. Accordingly, these studies involve extrapolation from a small number of homolog pairs to the entire chromosome population. Moreover, the progression of pairing is not observed in the same nucleus but must be inferred from different cells retrieved from the culture at different times. By contrast, different sensitivities to translation velocity thresholds of small, medium-sized, and very large chromosomes are readily captured by our model but would have eluded any population-based approach (see Fig. 6).

Conclusion

The modeling approach developed here suggests that homolog pairing is achieved by two temporally overlapping, yet mechanistically distinct processes: Homologs become confined to a nuclear area due to repulsive interactions with the entire non-homologous chromosome set. Confinement to smaller areas enables homologs to assess similarities by close-range physical DNA interactions. Our model is readily scaled to different biological settings and may provide predictions for a multitude of cellular scenarios, laying the groundwork for experimental studies. For example, meiosis in the Indian muntjac involves 3 homolog pairs, whereas in some insects and plants between 300 to 600 homolog pairs need to complete pairing [68,69]. Such complexities are inaccessible to current experimentation but become analyzable by the current model. Importantly, our model makes specific predictions about contributions of chromosome dimensions and movement velocity in combination with chromosome numbers that may further be affected by specific nuclear dimensions. Chromosome number, nuclear dimensions and movement speeds vary widely among different organisms and may affect pairing requirements. All three parameters are accessible to experimental manipulation [70], rendering predictions of our model testable in appropriate experimentation.

Supporting information

Effect of velocity on pairing kinetics

Similar to Fig. 3, we consider the effect of movement velocity on pairing kinetics. In particular, we observe that pairing kinetics are accelerated as velocity increases. Fig. S1 Figa is a reproduction of Fig. 6a showing how movement velocity changes the homolog pairing efficiency. Fig. S1 Figb, rescales each curve in (a) by the maximum pairing efficiency. The model predicts that the benefits associated with increased velocity appear to saturate past 300 nm/s. To investigate this trend's direct effect on pairing kinetics, we compute the distances between homologs as a function of chromosome movement speed. The results are summarized in Fig. S2 Figa-d. Accordingly, smaller compared to larger chromosomes require lower movement velocities for timely pairing completion.

S1 Fig. Effects of chromosome velocity on pairing kinetics. (a) Reproduction of Fig. 6a, each dot indicates the average pairing levels of all 32 chromosomes of true

sizes at the indicated time points. Black (300 nm/s) indicates pairing levels at the velocity of chromosome movements in the wild type model in Figs. 3-5 Chromosomes fail to pair at velocities around 150 nm/s, likely due to the effect of thermal noise. Increases in 30 nm/s increments increases pairing efficiencies at $t = 9h \sim 3$-fold, with more modest gains above 240 nm/s where essentially all 16 homologs pair efficiently. (b) Results from Fig. S1a were normalized by maximum pairing levels, as described for Fig. 3b. With increased movement velocities, 50% pairing levels are achieved at progressively earlier time points.

S2 Fig. Effects of movement velocity on homologous pairing kinetics. All results for 16 homolog pairs using true chromosome lengths. Chromosomes are arranged according to their initial distance to facilitate comparison with the experimental data set. Chromosome movement velocity is (a) 180 nm/s, (b) 210 nm/s, (c) 240 nm/s, and (d) 270 nm/s. Note the sharp transition between 210 nm/s and 240 nm/s, as also shown in Fig. 6a. The pairing distance is highlighted in gray at 400 nm. (200 realizations, error bars indicate SD).

Non-homologous chromosome distances in wild type compared to *spo11* hypomorph

The complementary plot to Fig. 7 shows the distribution of non-homologous pairing distances as a function of time. Fig. S3 Fig provides a direct comparison between non-homologous chromosome distances in wild type (a) and *spo11* hypomorph (b) where true chromosome lengths are used. Numerically, we tracked the distance between a given homolog and selected the non-homologous chromosome in the same nucleus with the closest initial distance to its homologous pair. The simulation then tracks the dynamics of both throughout time and we plot the distance between a given chromosome and the previously identified non-homologous chromosome. The results indicate that there is no bias in time for a chromosome with any non-homologous chromosome in the nucleus. Also, the results indicate that the mutation does not have a strong effect on non-homologous interactions as it only modifies their strength, but not their qualitative behavior of creating excluded regions. One difference as noted in Fig. 7 is that while both the wild type and mutant produce excluded regions, the strength of the repulsion in the wild type makes these regions more severe and drives homologous pairing to occur much faster. This validates the model in that the only different interaction occurs with a given chromosome's homologous mate (compare homologous results in Fig. 7 with non-homologous results in Fig. S3 Fig).

S3 Fig. Non-homologous chromosome distances for wild type and *spo11* hypomorph, with experimental observations in the insets. (a) Reproduction of Fig. 4b for non-homologous distances in the wild type simulations. (b) Non-homologous pairs of *spo11* mutants where one of the two homolog partners is matched with a non-homologous chromosome that exhibits an optimally matched initial distance with its cognate homolog partner at $t = 3h$. Inset in (b) shows experimentally determined distances between non-homologous GFP tagged chromosomes II and III. For details on the experimental conditions see [12]. The pairing distance is highlighted in gray at 400 nm. *Note the experimental data do not include information for $t = 9h$. (200 realizations, error bars indicate SD).

Illustration of the Effect of Repulsive (Non-homologous) and Attractive (Homologous) Forces on Local Chromosome Dynamics

S4 Fig. Non-homologous chromosome interactions of chromosomes in a cell nucleus. (a-f) Focus on the highlighted region where four non-homologous chromosomes interact over 30 seconds of real time. The transparent outer radius is the attractive force range, which does not affect this interaction, and the solid inner range is the repulsive force range. This demonstrates the short-range nature of the repulsive potential in the model. Only the purple and red chromosomes approach each other sufficiently close to experience repulsive forces sufficiently strong to affect their directions of movements. For full movie of this event see Supplemental Movie S1 Video.

S5 Fig. Homologous chromosome interactions of chromosomes in a cell nucleus.(a-f) Focus on the highlighted region where two homologous chromosomes interact over 10 seconds of real time. The transparent outer radius is the attractive force range, and the solid inner range is the repulsive force range, which has no effect in this interaction. This demonstrates the short-range attractive force is not a strong pull, but rather takes the close proximity of two homologs over time for the binding process to occur. The two chromosomes approach each other and once they are essentially overlapping and bound together the two chromosomes remain together for the remainder of time. For full movie of this event see Supplemental Movie S1 Video.

Effect of a too strong attraction force on chromosome kinetics

S6 Fig. Effects of chromosome size on pairing kinetics and efficiency with strong attractive force. Average distances over time between homolog pairs where repulsive and attractive radii are adjusted proportionally to the sizes of actual yeast chromosomes. Here C_a is 100 times larger than in Table 1 and C_r is 100 times smaller simulating a strong attractive force between chromosomes and a very weak repulsion force. Observe that pairing occurs on a much smaller timescale than observed in the experiment and the three smallest chromosomes essentially never pair over 200 realizations.

Supplemental movie files

Movie files are available at a dedicated online Zenodo Repository:
`https://zenodo.org/record/7415620#.Y82hJi-B2fV`

S1 Video. WT Chromosome Trajectories during Prophase I. The movie shows one realization of the agent-based model. The simulation movie covers the homology search process from $t = 3h$ to $t = 9h$. Matching colors correspond to homologous pairs. True chromosome lengths are incorporated and scale the relevant interaction radii. The outer radius represents the weak attractive region, and the inner radius represents the non-homologous repulsive region.

S2 Video. spo11 hypomorph (30% WT DSB levels) Chromosome Trajectories during Prophase I (parameters from Fig. 7b). The movie depicts one realization of the agent-based model for the *spo11* hypomorphic mutant. The simulation movie covers the homology search process from $t = 3h$ to $t = 9h$ where mutant *spo11* is associated with a weaker attractive force as well as the translation velocity being reduced to 77% of wild type velocity v_0. True chromosome lengths are incorporated and scale the relevant interaction radii. Matching colors correspond to homologous pairs. The outer and inner radii represent the homologous attractive and

the non-homologous repulsive regions, respectively. Note that the reduction in velocity delays homologous pairing consistent with experimental observations in [12].

Acknowledgments

The work of S.R. was supported by the CSU Center for Applied Data Analysis and Modeling (ADAM). AC and SR developed the mathematical model and carried out numerical simulations, emerging from discussion with GVB. AC, GVB, and SR analyzed the results and wrote the manuscript.

References

1. Xu N, Tsai CL, Lee JT. Transient homologous chromosome pairing marks the onset of X inactivation. Science. 2006;311(5764):1149–1152.
2. LaSalle JM, Lalande M. Homologous association of oppositely imprinted chromosomal domains. Science. 1996;272(5262):725–728.
3. Gruhn JR, Hoffmann ER. Errors of the Egg: The Establishment and Progression of Human Aneuploidy Research in the Maternal Germline. Annual Review of Genetics. 2022;56:369–390.
4. Lam I, Keeney S. Mechanism and regulation of meiotic recombination initiation. Cold Spring Harbor perspectives in biology. 2015;7(1):a016634.
5. Barzel A, Kupiec M. Finding a match: how do homologous sequences get together for recombination? Nature Reviews Genetics. 2008;9(1):27–37.
6. Zickler D, Kleckner N. Recombination, pairing, and synapsis of homologs during meiosis. Cold Spring Harbor perspectives in biology. 2015;7(6):a016626.
7. Lefrançois P, Rockmill B, Xie P, Roeder GS, Snyder M. Multiple pairwise analysis of non-homologous centromere coupling reveals preferential chromosome size-dependent interactions and a role for bouquet formation in establishing the interaction pattern. PLoS Genetics. 2016;12(10):e1006347.
8. Sym M, Engebrecht J, Roeder GS. ZIP1 is a synaptonemal complex protein required for meiotic chromosome synapsis. Cell. 1993;72(3):365–378.
9. Storlazzi A, Gargano S, Ruprich-Robert G, Falque M, David M, Kleckner N, et al. Recombination proteins mediate meiotic spatial chromosome organization and pairing. Cell. 2010;141(1):94–106.
10. Weiner BM, Kleckner N. Chromosome pairing via multiple interstitial interactions before and during meiosis in yeast. Cell. 1994;77(7):977–991.
11. Burgess SM, Kleckner N, Weiner BM. Somatic pairing of homologs in budding yeast: existence and modulation. Genes & development. 1999;13(12):1627–1641.
12. Sandhu R, Neria FM, Neria JM, Chen X, Hollingsworth NM, Börner GV. DNA helicase Mph1FANCM ensures meiotic recombination between parental chromosomes by dissociating precocious displacement loops. Developmental cell. 2020;53(4):458–472.

13. Brown MS, Zanders S, Alani E. Sustained and rapid chromosome movements are critical for chromosome pairing and meiotic progression in budding yeast. Genetics. 2011;188(1):21–32.

14. Conrad MN, Lee CY, Chao G, Shinohara M, Kosaka H, Shinohara A, et al. Rapid telomere movement in meiotic prophase is promoted by NDJ1, MPS3, and CSM4 and is modulated by recombination. Cell. 2008;133(7):1175–1187.

15. Koszul R, Kim K, Prentiss M, Kleckner N, Kameoka S. Meiotic chromosomes move by linkage to dynamic actin cables with transduction of force through the nuclear envelope. Cell. 2008;133(7):1188–1201.

16. Brar GA, Hochwagen A, Ee LsS, Amon A. The multiple roles of cohesin in meiotic chromosome morphogenesis and pairing. Molecular Biology of the Cell. 2009;20(3):1030–1047.

17. Peoples-Holst TL, Burgess SM. Multiple branches of the meiotic recombination pathway contribute independently to homolog pairing and stable juxtaposition during meiosis in budding yeast. Genes & development. 2005;19(7):863–874.

18. Padmore R, Cao L, Kleckner N. Temporal comparison of recombination and synaptonemal complex formation during meiosis in S. cerevisiae. Cell. 1991;66(6):1239–1256.

19. Newman TA, Beltran B, McGehee JM, Elnatan D, Cahoon CK, Paddy MR, et al. Diffusion and distal linkages govern interchromosomal dynamics during meiotic prophase. Proceedings of the National Academy of Sciences. 2022;119(12):e2115883119.

20. Neale MJ, Ramachandran M, Trelles-Sticken E, Scherthan H, Goldman AS. Wild-type levels of Spo11-induced DSBs are required for normal single-strand resection during meiosis. Molecular cell. 2002;9(4):835–846.

21. Marshall WF, Fung JC. Modeling meiotic chromosome pairing: nuclear envelope attachment, telomere-led active random motion, and anomalous diffusion. Physical biology. 2016;13(2):026003.

22. Marshall WF, Fung JC. Modeling meiotic chromosome pairing: a tug of war between telomere forces and a pairing-based Brownian ratchet leads to increased pairing fidelity. Physical biology. 2019;16(4):046005.

23. Penfold CA, Brown PE, Lawrence ND, Goldman AS. Modeling meiotic chromosomes indicates a size dependent contribution of telomere clustering and chromosome rigidity to homologue juxtaposition. PLoS computational biology. 2012;8(5):e1002496.

24. Navarro EJ, Marshall WF, Fung JC. Modeling cell biological features of meiotic chromosome pairing to study interlock resolution. PLoS Computational Biology. 2022;18(6):e1010252.

25. Dorninger D, Karigl G, Loidl J. Simulation of chromosomal homology searching in meiotic pairing. Journal of theoretical biology. 1995;176(2):247–260.

26. Ryan SD, Berlyand L, Haines BM, Karpeev D. A kinetic model for semidilute bacterial suspensions. Multiscale Modeling & Simulation. 2013;11(4):1176–1196.

27. Ryan SD. Role of hydrodynamic interactions in chemotaxis of bacterial populations. Physical biology. 2019;17(1):016003.

28. D'Orsogna MR, Chuang YL, Bertozzi AL, Chayes LS. Self-propelled particles with soft-core interactions: patterns, stability, and collapse. Physical review letters. 2006;96(10):104302.

29. Alleva B, Smolikove S. Moving and stopping: Regulation of chromosome movement to promote meiotic chromosome pairing and synapsis. Nucleus. 2017;8(6):613–624.

30. Spichal M, Fabre E. The emerging role of the cytoskeleton in chromosome dynamics. Frontiers in genetics. 2017;8:60.

31. Ariel G, Sidortsov M, Ryan SD, Heidenreich S, Bär M, Be'Er A. Collective dynamics of two-dimensional swimming bacteria: Experiments and models. Physical Review E. 2018;98(3):032415.

32. Wang F, Yuan J, Berg HC. Switching dynamics of the bacterial flagellar motor near zero load. Proceedings of the National Academy of Sciences. 2014;111(44):15752–15755.

33. Brosseau Q, Usabiaga FB, Lushi E, Wu Y, Ristroph L, Zhang J, et al. Relating rheotaxis and hydrodynamic actuation using asymmetric gold-platinum phoretic rods. Physical review letters. 2019;123(17):178004.

34. Drescher K, Dunkel J, Cisneros LH, Ganguly S, Goldstein RE. Fluid dynamics and noise in bacterial cell–cell and cell–surface scattering. Proceedings of the National Academy of Sciences. 2011;108(27):10940–10945.

35. Issa MW, Baumgartner NR, Kalil MA, Ryan SD, Wirth CL. Charged nanoparticles quench the propulsion of active janus colloids. ACS omega. 2019;4(8):13034–13041.

36. Chepizhko O, Saintillan D, Peruani F. Revisiting the emergence of order in active matter. Soft Matter. 2021;17(11):3113–3120.

37. Lawley SD, Miles CE. Diffusive search for diffusing targets with fluctuating diffusivity and gating. Journal of Nonlinear Science. 2019;29(6):2955–2985.

38. Hunter N, Chambers SR, Louis EJ, Borts RH. The mismatch repair system contributes to meiotic sterility in an interspecific yeast hybrid. The EMBO journal. 1996;15(7):1726–1733.

39. Tsubouchi H, Roeder GS. The importance of genetic recombination for fidelity of chromosome pairing in meiosis. Developmental cell. 2003;5(6):915–925.

40. Smith SB, Cui Y, Bustamante C. Overstretching B-DNA: the elastic response of individual double-stranded and single-stranded DNA molecules. Science. 1996;271(5250):795–799.

41. Mimitou EP, Yamada S, Keeney S. A global view of meiotic double-strand break end resection. Science. 2017;355(6320):40–45.

42. Lee CY, Conrad MN, Dresser ME. Meiotic chromosome pairing is promoted by telomere-led chromosome movements independent of bouquet formation. PLoS genetics. 2012;8(5):e1002730.

43. Marshall W, Straight A, Marko J, Swedlow J, Dernburg A, Belmont A, et al. Interphase chromosomes undergo constrained diffusional motion in living cells. Current Biology. 1997;7(12):930–939.

44. MATLAB. version 9.11.0.1809720 (R2021b). Natick, Massachusetts: The MathWorks Inc.; 2021.

45. Ryan SD. GitHub Repository: Chromosome Dynamics in Prophase I; 2023. Available from: `44.https://github.com/sdryan/ChromosomeDynamicsProphase1`.

46. Murakami H, Lam I, Huang PC, Song J, van Overbeek M, Keeney S. Multilayered mechanisms ensure that short chromosomes recombine in meiosis. Nature. 2020;582(7810):124–128.

47. Kaback DB, Guacci V, Barber D, Mahon JW. Chromosome size-dependent control of meiotic recombination. Science. 1992;256(5054):228–232.

48. Therizols P, Duong T, Dujon B, Zimmer C, Fabre E. Chromosome arm length and nuclear constraints determine the dynamic relationship of yeast subtelomeres. Proceedings of the National Academy of Sciences. 2010;107(5):2025–2030.

49. Wong H, Arbona JM, Zimmer C. How to build a yeast nucleus. Nucleus. 2013;4(5):361–366.

50. Marko JF, Siggia ED. Polymer models of meiotic and mitotic chromosomes. Molecular biology of the cell. 1997;8(11):2217–2231.

51. Cheng TM, Heeger S, Chaleil RA, Matthews N, Stewart A, Wright J, et al. A simple biophysical model emulates budding yeast chromosome condensation. Elife. 2015;4:e05565.

52. Ariel G, Ayali A. Locust collective motion and its modeling. PLOS computational Biology. 2015;11(12):e1004522.

53. Boissard E, Degond P, Motsch S. Trail formation based on directed pheromone deposition. Journal of mathematical biology. 2013;66:1267–1301.

54. Ryan SD. A model for collective dynamics in ant raids. Journal of mathematical biology. 2016;72:1579–1606.

55. Baumgartner II NR, Ryan SD. Interaction of red crabs with yellow crazy ants during migration on Christmas Island. Mathematical Biosciences. 2020;330:108486.

56. Ryan SD, McCarthy Z, Potomkin M. Motor protein transport along inhomogeneous microtubules. Bulletin of Mathematical Biology. 2021;83:1–29.

57. Ryan SD, Haines BM, Berlyand L, Ziebert F, Aranson IS. Viscosity of bacterial suspensions: Hydrodynamic interactions and self-induced noise. Physical Review E. 2011;83(5):050904.

58. Ryan SD, Ariel G, Be'er A. Anomalous fluctuations in the orientation and velocity of swarming bacteria. Biophysical journal. 2016;111(1):247–255.

59. Peled S, Ryan SD, Heidenreich S, Bär M, Ariel G, Be'Er A. Heterogeneous bacterial swarms with mixed lengths. Physical Review E. 2021;103(3):032413.

60. Leu JY, Chua PR, Roeder GS. The meiosis-specific Hop2 protein of S. cerevisiae ensures synapsis between homologous chromosomes. Cell. 1998;94(3):375–386.

61. Zierhut C, Berlinger M, Rupp C, Shinohara A, Klein F. Mnd1 is required for meiotic interhomolog repair. Current Biology. 2004;14(9):752–762.

62. Petukhova GV, Romanienko PJ, Camerini-Otero RD. The Hop2 protein has a direct role in promoting interhomolog interactions during mouse meiosis. Developmental cell. 2003;5(6):927–936.

63. Kerzendorfer C, Vignard J, Pedrosa-Harand A, Siwiec T, Akimcheva S, Jolivet S, et al. The Arabidopsis thaliana MND1 homologue plays a key role in meiotic homologous pairing, synapsis and recombination. Journal of Cell Science. 2006;119(12):2486–2496.

64. Petukhova GV, Pezza RJ, Vanevski F, Ploquin M, Masson JY, Camerini-Otero RD. The Hop2 and Mnd1 proteins act in concert with Rad51 and Dmc1 in meiotic recombination. Nature structural & molecular biology. 2005;12(5):449–453.

65. Griffiths S, Sharp R, Foote TN, Bertin I, Wanous M, Reader S, et al. Molecular characterization of Ph1 as a major chromosome pairing locus in polyploid wheat. Nature. 2006;439(7077):749–752.

66. Bozdag GO, Ono J, Denton JA, Karakoc E, Hunter N, Leu JY, et al. Breaking a species barrier by enabling hybrid recombination. Current biology. 2021;31(4):R180–R181.

67. Scherthan H, Weich S, Schwegler H, Heyting C, Härle M, Cremer T. Centromere and telomere movements during early meiotic prophase of mouse and man are associated with the onset of chromosome pairing. The Journal of Cell Biology. 1996;134(5):1109–1125.

68. Brown RC, Lemmon B. Sporogenesis in eusporangiate ferns: II. Polyplastidic meiosis in Ophioglossum (Ophioglossales). Journal of Plant Research. 2001;114:237–246.

69. Lukhtanov VA. The blue butterfly Polyommatus (Plebicula) atlanticus (Lepidoptera, Lycaenidae) holds the record of the highest number of chromosomes in the non-polyploid eukaryotic organisms. Comparative Cytogenetics. 2015;9(4):683.

70. Richardson SM, Mitchell LA, Stracquadanio G, Yang K, Dymond JS, DiCarlo JE, et al. Design of a synthetic yeast genome. Science. 2017;355(6329):1040–1044.

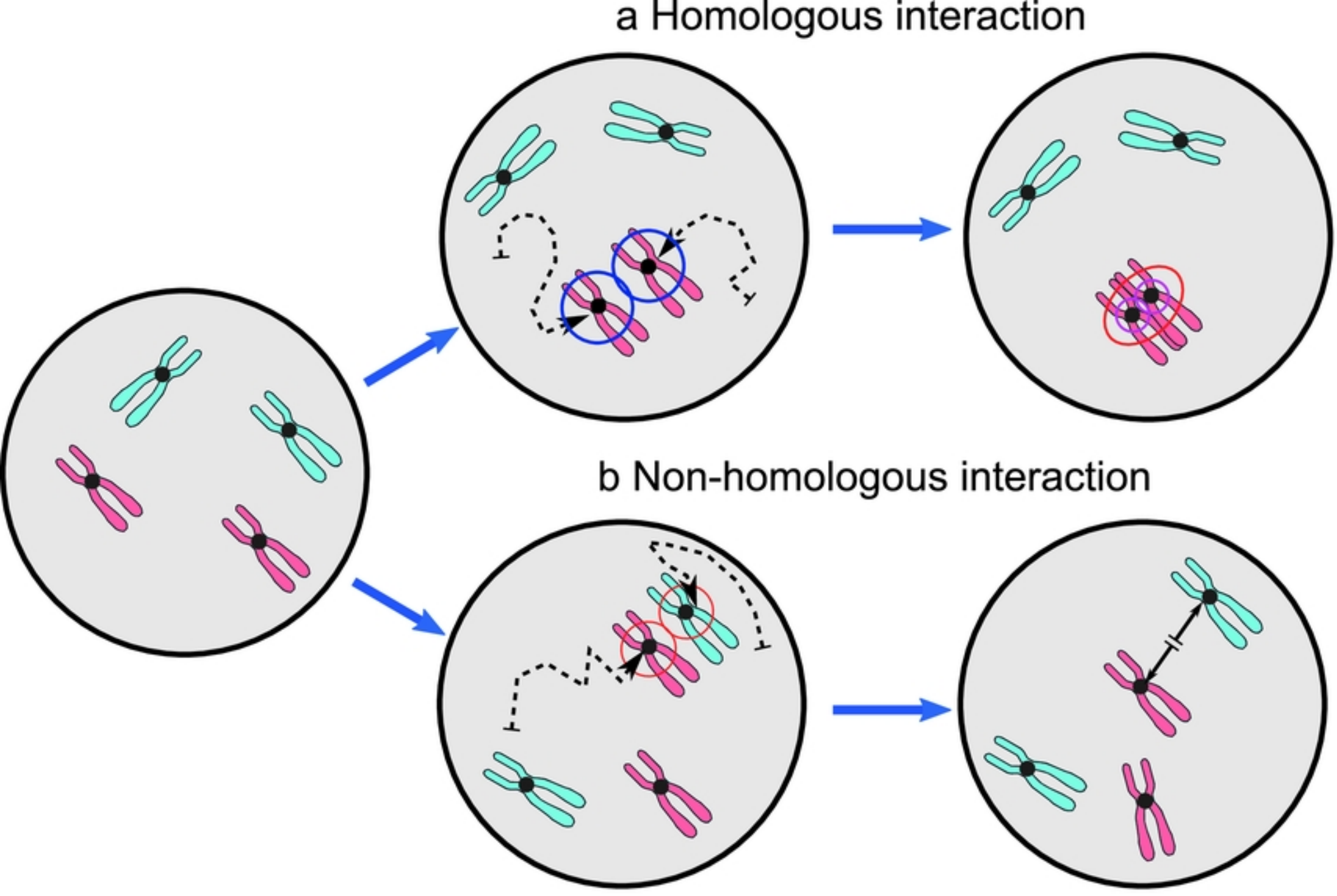

$$\dot{\mathbf{x}}_i = \overbrace{v_0 \mathbf{d}_i}^{Translation} + \overbrace{\sum_{i \neq j}^{N} \mathbf{F}^j(\mathbf{x}_i - \mathbf{x}_j)}^{Interaction} + \overbrace{\sqrt{2D}\dot{\mathbf{W}}}^{Noise} \quad (1)$$

$$\mathbf{F}^j(\mathbf{x}_i - \mathbf{x}_j) = -\nabla U(\mathbf{x}_i - \mathbf{x}_j) \quad (2)$$

$$U(\mathbf{x}_i - \mathbf{x}_j) = \begin{cases} C_r e^{-\frac{|\mathbf{x}_i - \mathbf{x}_j|}{\ell_{r_1}}} - C_a e^{-\frac{|\mathbf{x}_i - \mathbf{x}_j|}{\ell_a}}, & j \text{ hom.}, \\ C_r e^{-\frac{|\mathbf{x}_i - \mathbf{x}_j|}{\ell_{r_1}}} + C_r e^{-\frac{|\mathbf{x}_i - \mathbf{x}_j|}{\ell_r}}, & j \text{ nhom.} \end{cases} \quad (3)$$

Figure 1

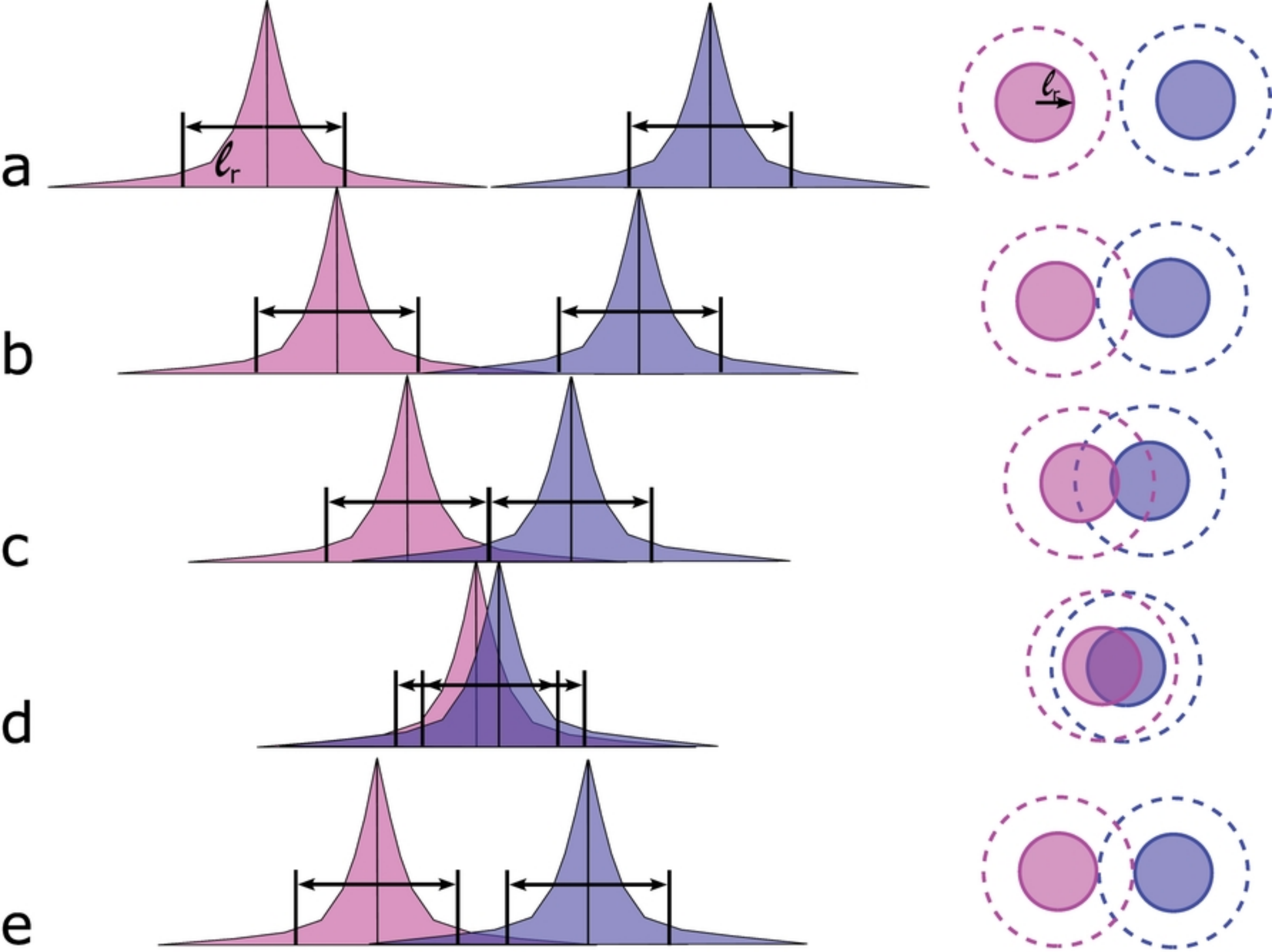

Figure 2

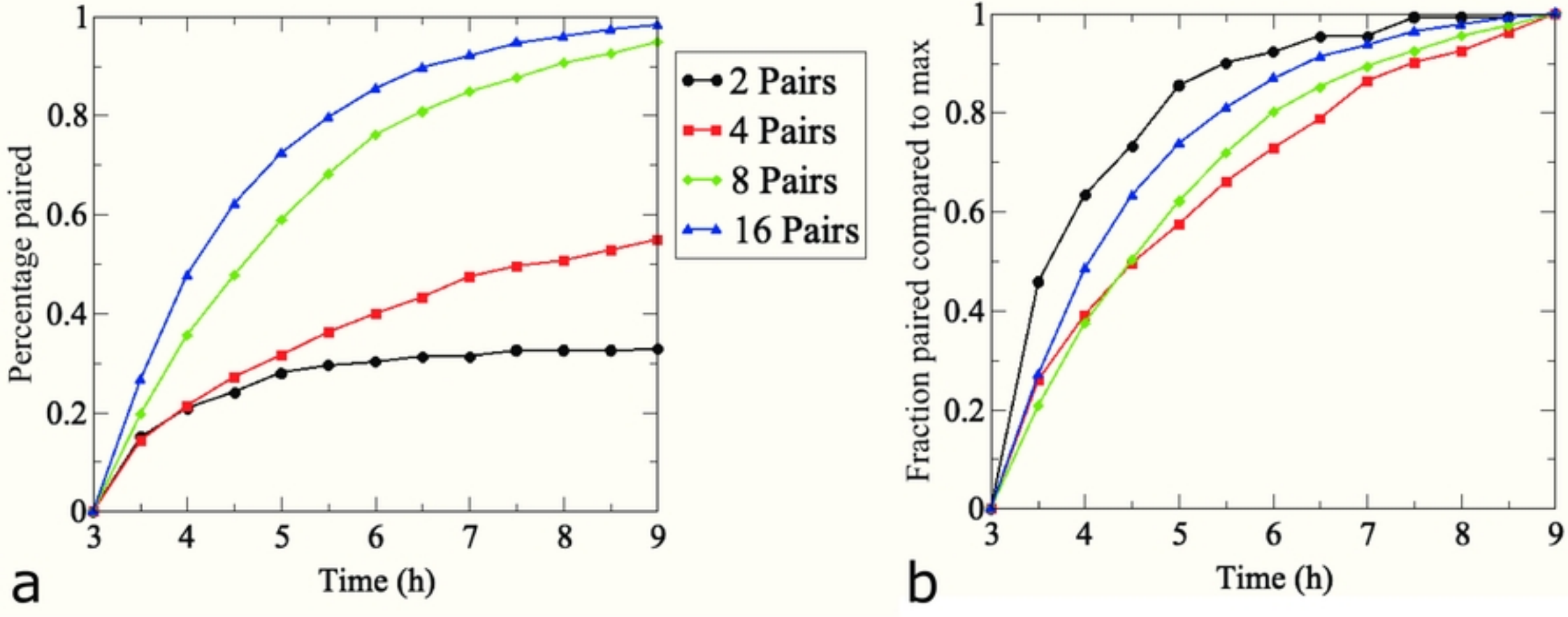
Percentage paired
Time (h)
2 Pairs
4 Pairs
8 Pairs
16 Pairs
a
Fraction paired compared to max
Time (h)
b

Figure 3

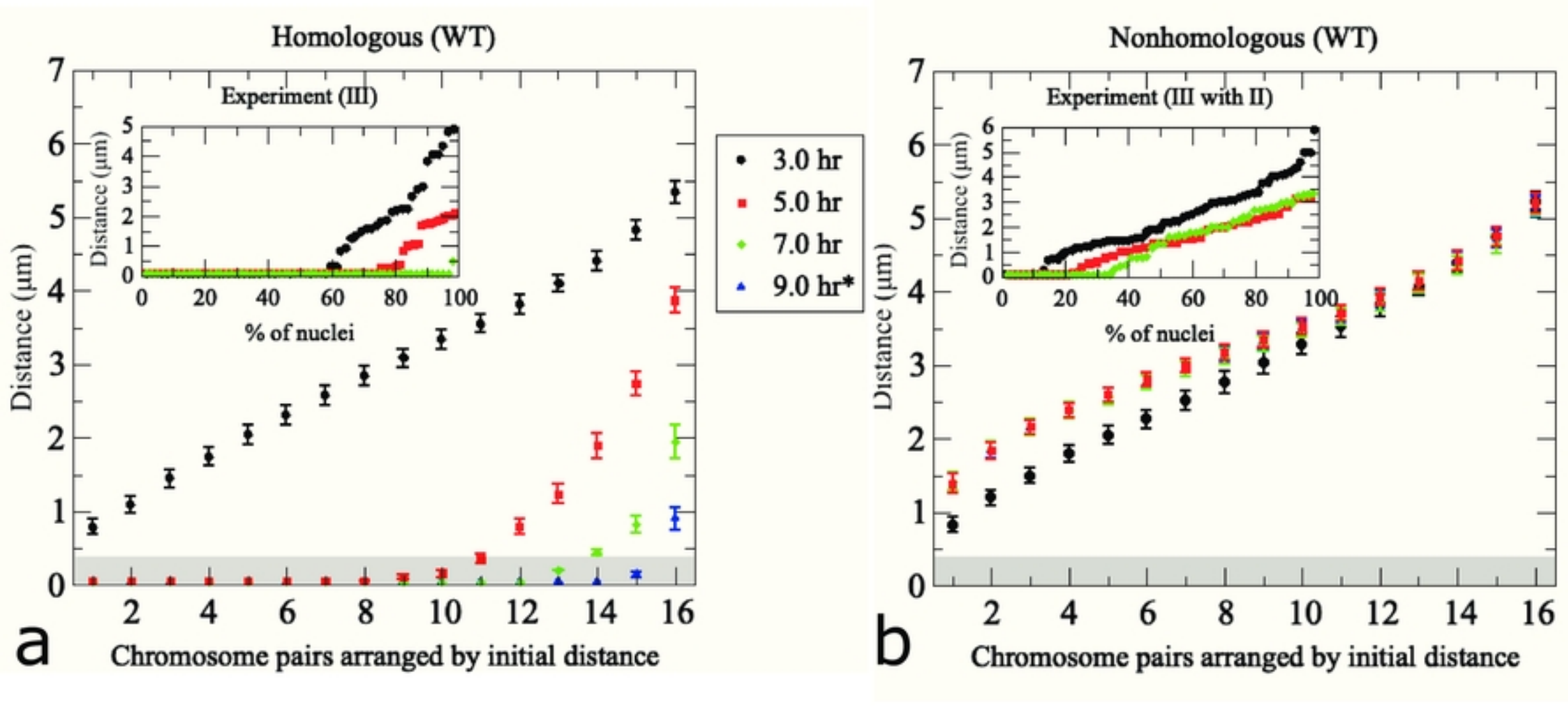
Homologous (WT)
Experiment (III)
Distance (μm)
% of nuclei
3.0 hr
5.0 hr
7.0 hr
9.0 hr*
a
Chromosome pairs arranged by initial distance
Nonhomologous (WT)
Experiment (III with II)
Distance (μm)
% of nuclei
b
Chromosome pairs arranged by initial distance

Figure 4

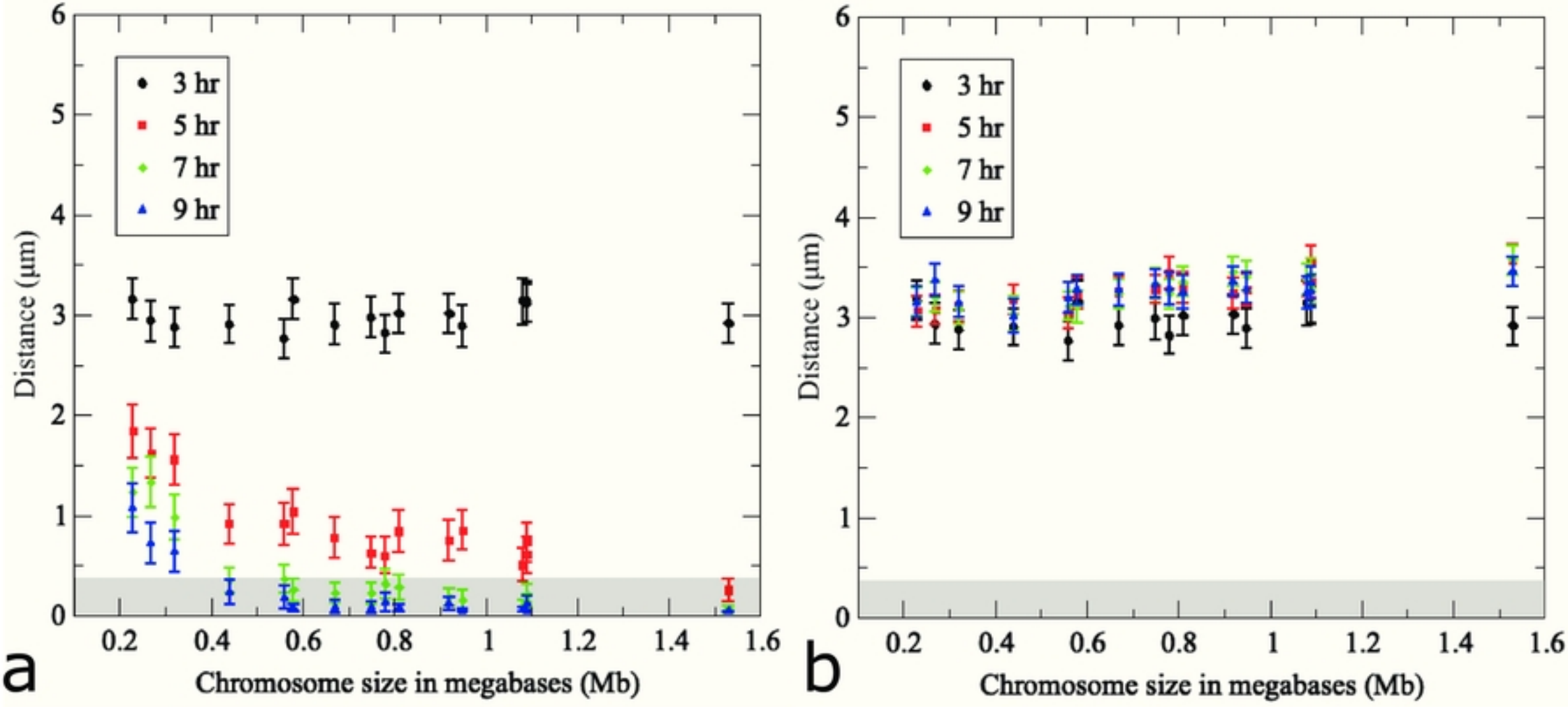
a
b
3 hr
5 hr
7 hr
9 hr
Distance (μm)
Chromosome size in megabases (Mb)
0
1
2
3
4
5
6
0.2
0.4
0.6
0.8
1
1.2
1.4
1.6

Figure 5

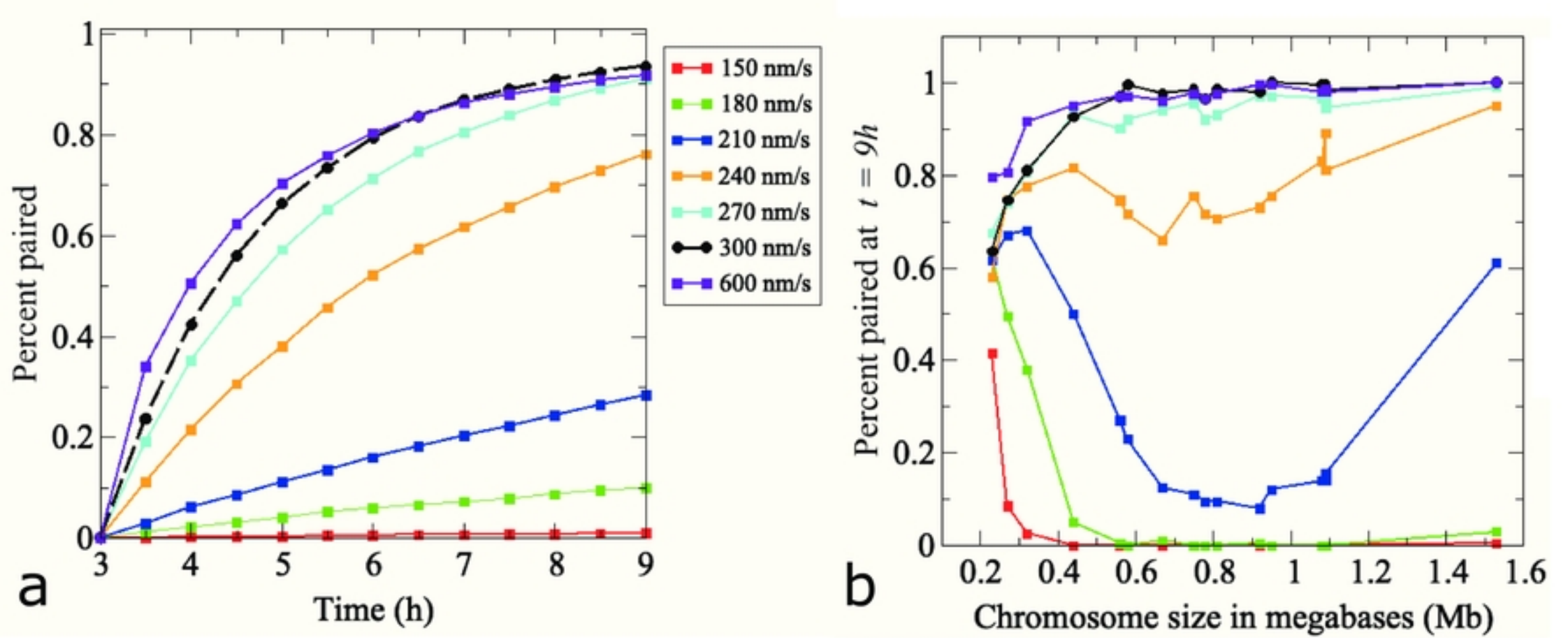
a
Percent paired
Time (h)
150 nm/s
180 nm/s
210 nm/s
240 nm/s
270 nm/s
300 nm/s
600 nm/s
b
Percent paired at $t = 9h$
Chromosome size in megabases (Mb)

Figure 6

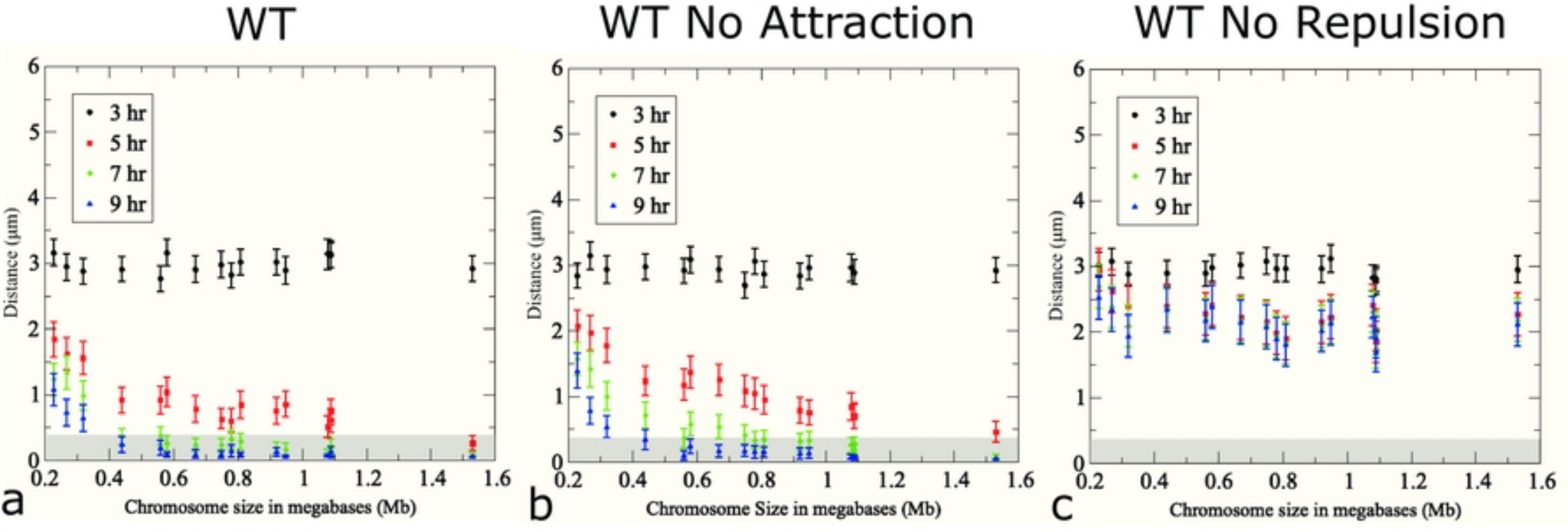
WT
WT No Attraction
WT No Repulsion
3 hr
5 hr
7 hr
9 hr
Distance (μm)
Chromosome size in megabases (Mb)
Chromosome Size in megabases (Mb)
a
b
c

Figure 7

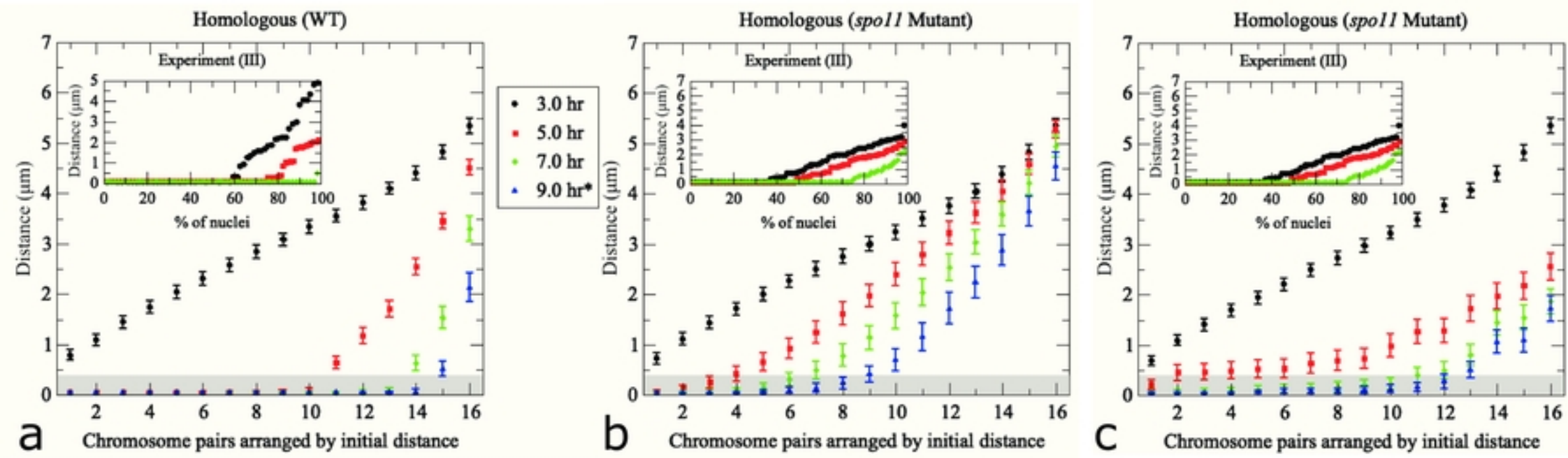
Homologous (WT)
Homologous (spo11 Mutant)
Homologous (spo11 Mutant)
Experiment (III)
Distance (μm)
% of nuclei
Chromosome pairs arranged by initial distance
3.0 hr
5.0 hr
7.0 hr
9.0 hr*
a
b
c

Figure 8

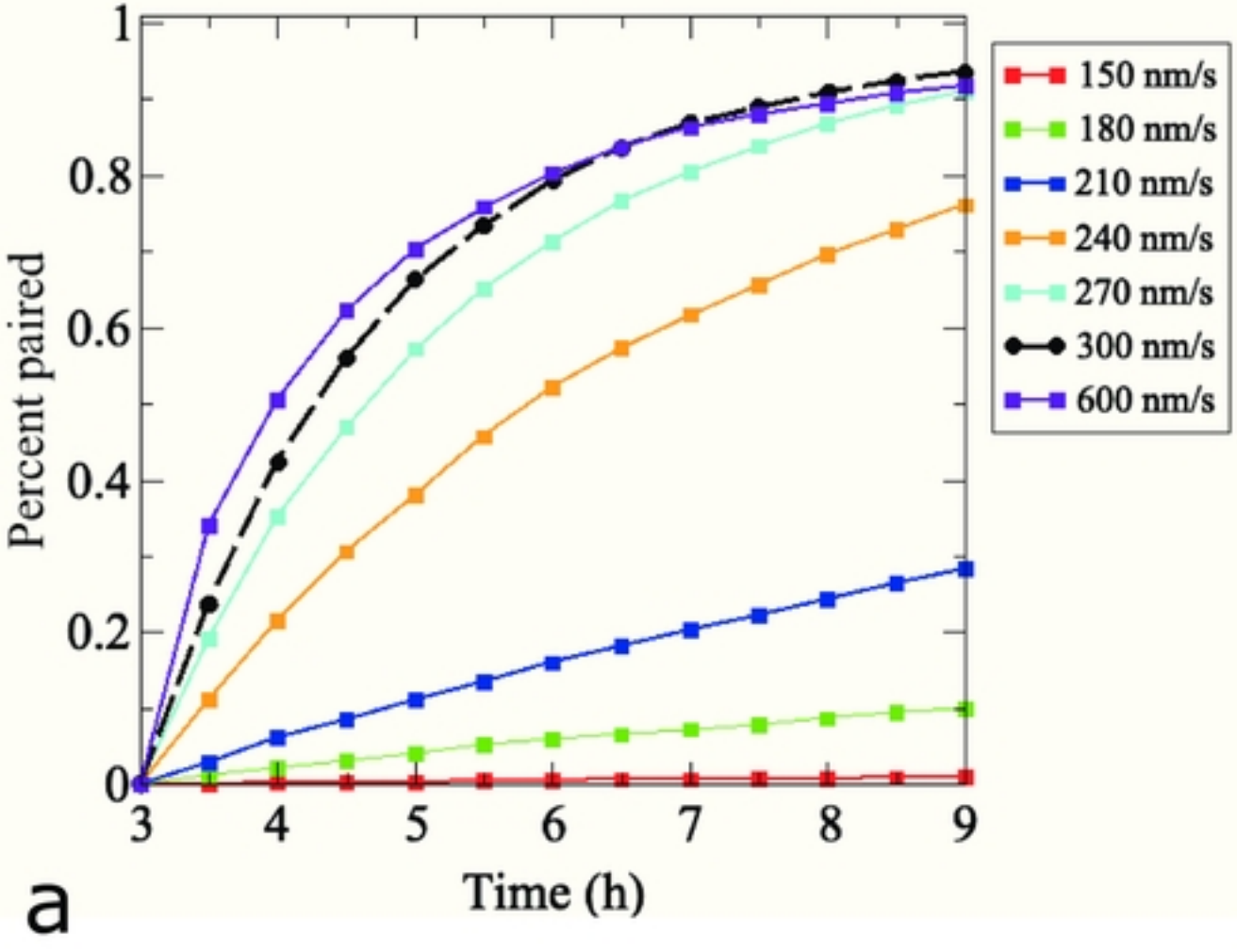
Percent paired
Time (h)
150 nm/s
180 nm/s
210 nm/s
240 nm/s
270 nm/s
300 nm/s
600 nm/s
a

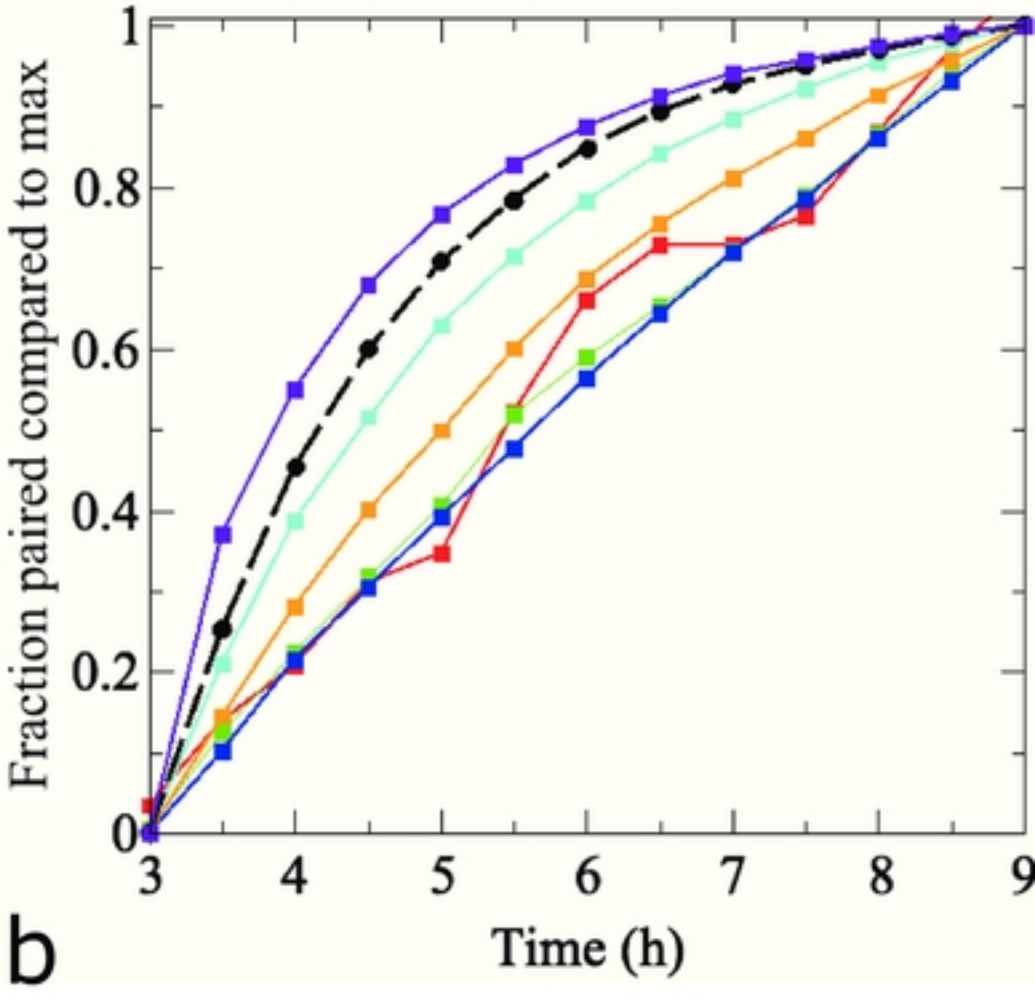
Fraction paired compared to max
Time (h)
b

SI Figure 1

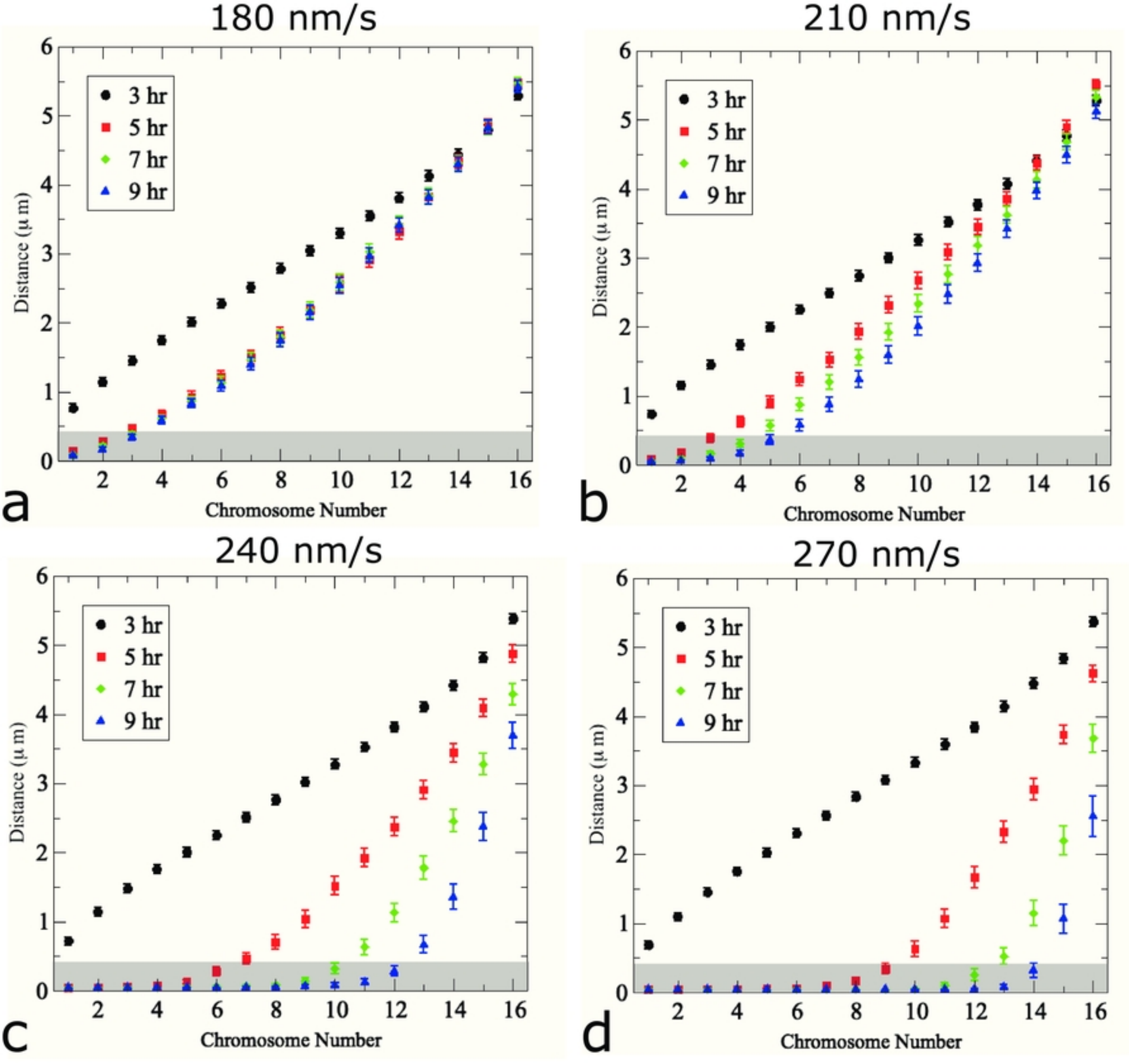
180 nm/s
210 nm/s
240 nm/s
270 nm/s
3 hr
5 hr
7 hr
9 hr
Distance (μ m)
Chromosome Number
a
b
c
d

SI Figure 2

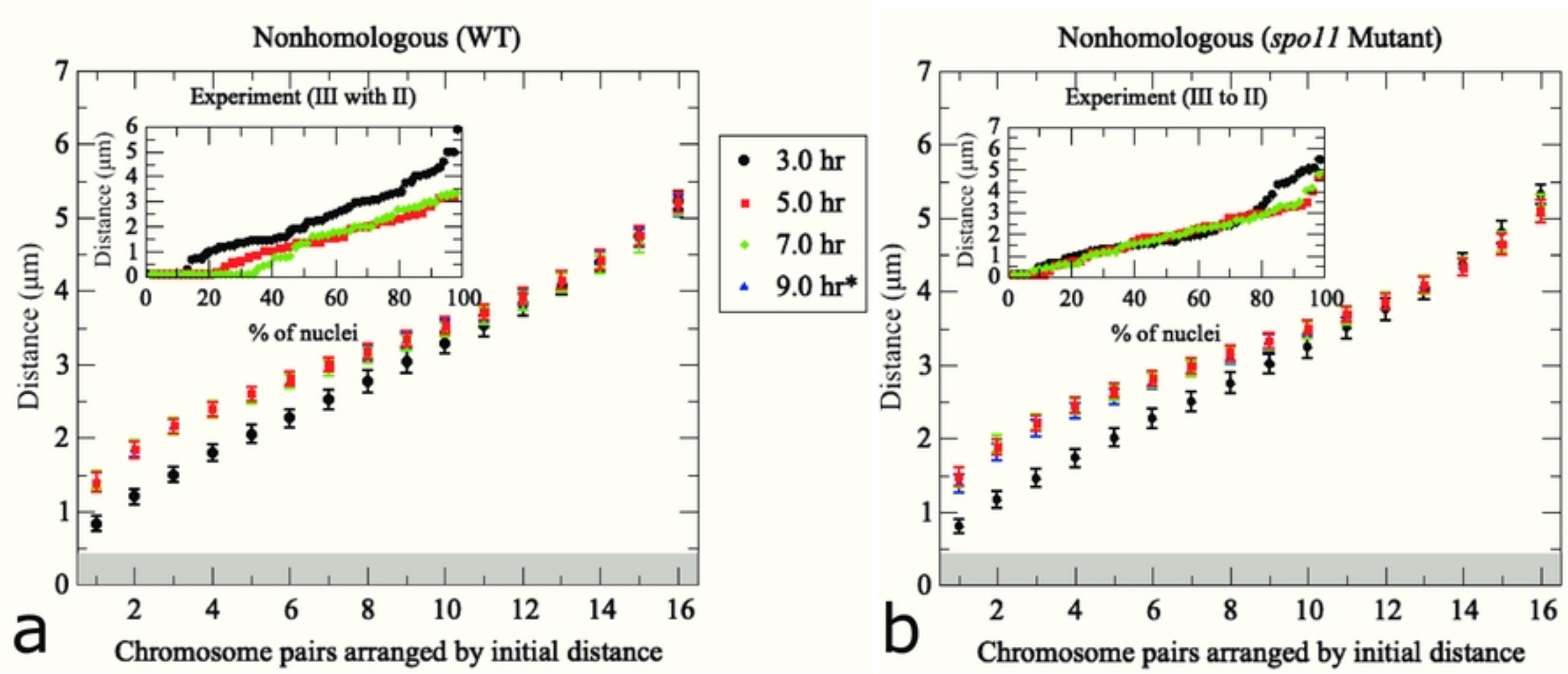
Nonhomologous (WT)
Experiment (III with II)
Distance (μm)
% of nuclei
3.0 hr
5.0 hr
7.0 hr
9.0 hr*
a
Chromosome pairs arranged by initial distance
Nonhomologous (spo11 Mutant)
Experiment (III to II)
Distance (μm)
% of nuclei
b
Chromosome pairs arranged by initial distance

SI Figure 3

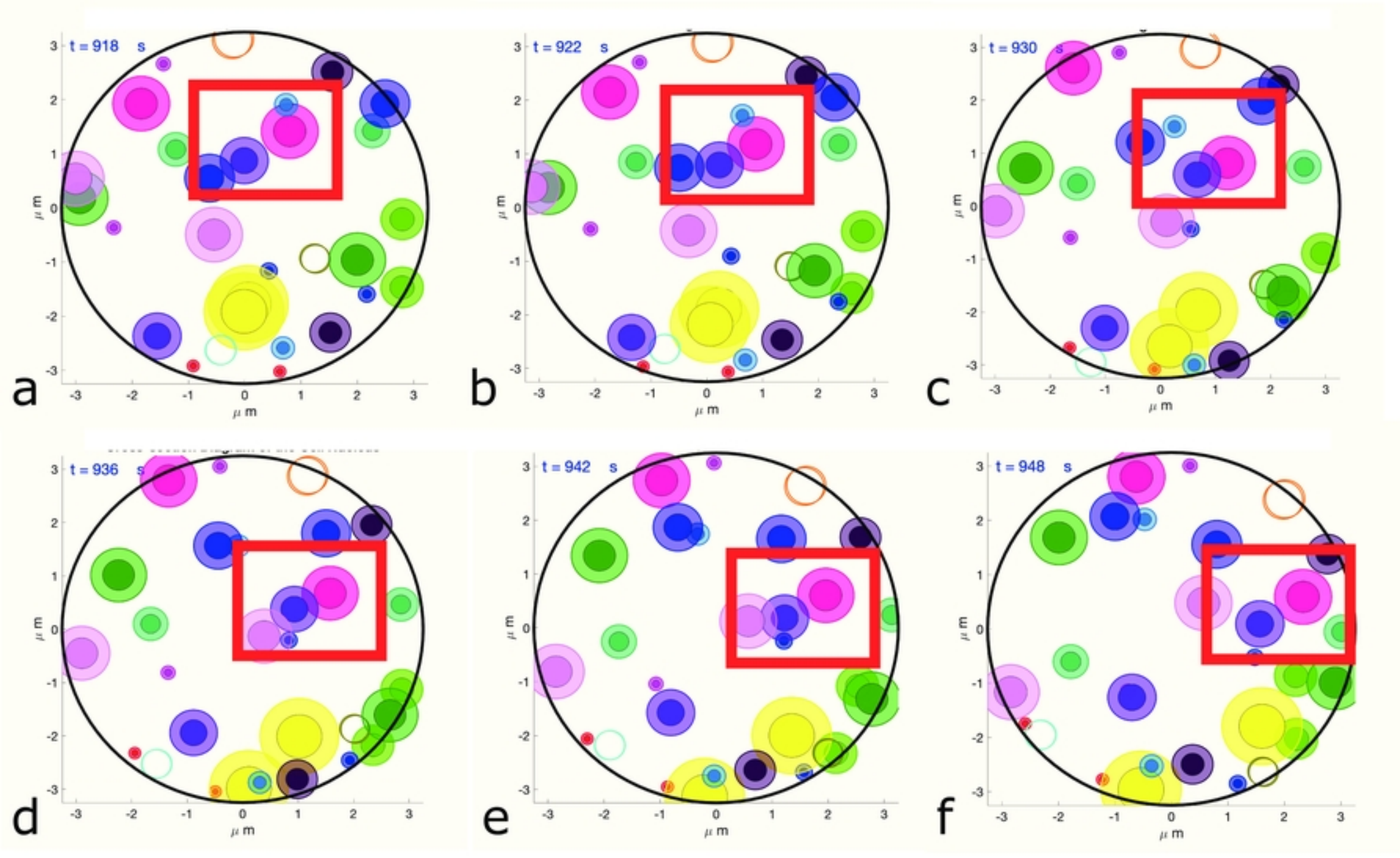

SI Figure 4

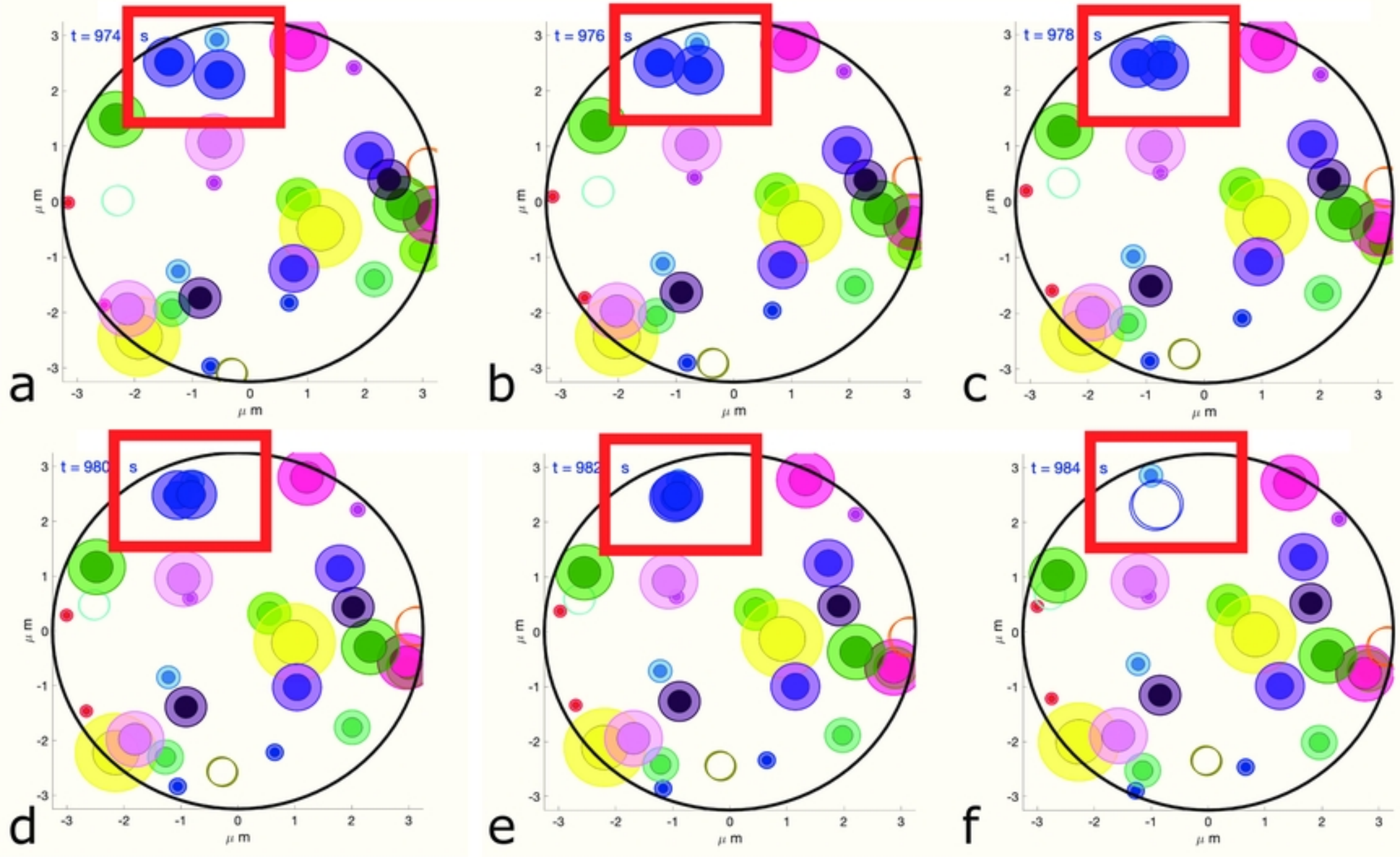

SI Figure 5

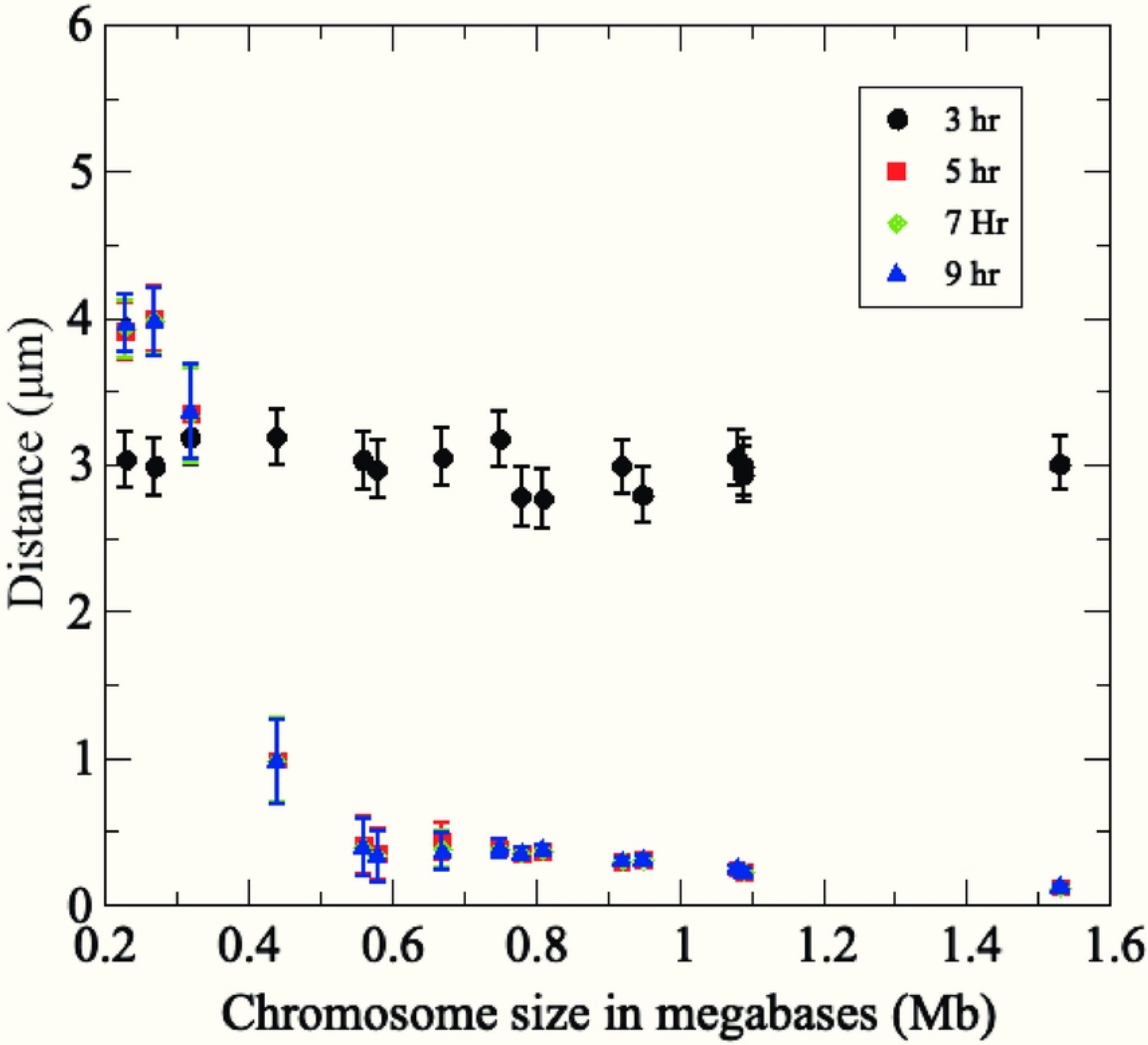
3 hr
5 hr
7 Hr
9 hr
Distance (μm)
Chromosome size in megabases (Mb)
0
1
2
3
4
5
6
0.2
0.4
0.6
0.8
1
1.2
1.4
1.6

SI Figure 6